Author Manuscript

Author Manuscript

Author Manuscript

Author Manuscript

HHS Public Access

Author manuscript

Nat Neurosci. Author manuscript; available in PMC 2021 January 13.

Published in final edited form as:

Nat Neurosci. 2020 September ; 23(9): 1067–1078. doi:10.1038/s41593-020-0672-0.

The endogenous neuronal complement inhibitor SRPX2 protects against complement-mediated synapse elimination during development

Qifei Cong[1,3], **Breeanne M. Soteros**[1,3], **Mackenna Wollet**[2], **Jun Hee Kim**[2], **Gek-Ming Sia**[1,*]

[1]Department of Pharmacology, University of Texas Health Science Center at San Antonio, San Antonio, TX 78229

[2]Department of Cellular and Integrative Physiology, University of Texas Health Science Center at San Antonio, San Antonio, TX 78229

Abstract

Complement-mediated synapse elimination has emerged as an important process in both brain development and neurological diseases, but whether neurons express complement inhibitors that protect synapses against complement-mediated synapse elimination remains unknown. Here, we show that the sushi domain protein SRPX2 is a neuronally expressed complement inhibitor that regulates complement-dependent synapse elimination. SRPX2 directly binds to C1q and blocks its activity, and $SRPX2^{-/Y}$ mice show increased C3 deposition and microglial synapse engulfment. They also show a transient decrease in synapse numbers and increase in retinogeniculate axon segregation in the lateral geniculate nucleus. In the somatosensory cortex, $SRPX2^{-/Y}$ mice show decreased thalamocortical synapse numbers and increased spine pruning. Dual $C3^{-/-}$;$SRPX2^{-/Y}$ mice exhibit phenotypes associated with $C3^{-/-}$ mice rather than $SRPX2^{-/Y}$ mice, indicating that C3 is necessary for SRPX2's effect on synapse elimination. Together, these results show that SRPX2 protects synapses against complement-mediated elimination in both the thalamus and the cortex.

INTRODUCTION

The proper regulation of synapse density during brain development is necessary for normal brain function, which requires a precise balance between synapse formation and elimination. During brain development, an excess of synapses is initially formed, and synapses are then selectively eliminated to sculpt mature circuits in the adult brain. Abnormalities in the processes of synapse formation and elimination have been linked to the pathogenesis of

Users may view, print, copy, and download text and data-mine the content in such documents, for the purposes of academic research, subject always to the full Conditions of use:http://www.nature.com/authors/editorial_policies/license.html#terms

*Corresponding author: siag@uthscsa.edu.

[3]These authors contributed equally to this work.

AUTHOR CONTRIBUTIONS

Q.C. and B.M.S. conducted the experiments; G.M.S. generated the SRPX2 transgenic mice, designed the experiments and wrote the manuscript. M.W. and J.H.K. performed the electrophysiology experiments.

DECLARATION OF INTERESTS

The authors declare no competing interests.

Author Manuscript Author Manuscript Author Manuscript Author Manuscript

several neurological disorders[1], indicating the importance of uncovering the molecular mechanisms involved.

The complement cascade of the innate immune system has recently emerged as an important mediator of synapse elimination during both brain development and neurological diseases. C1q activity causes deposition of C3 onto synapses[2], which in turn binds to CR3 on microglia and induces microglial engulfment of opsonized synapses[3]. Mice lacking C1QA or C3 show incomplete segregation of retinal ganglion cell (RGC) inputs to the visual thalamus[2], and C1QA knockout mice show enhanced synaptic connectivity and epileptiform activity in the neocortex[4]. Deletion of C1QA or C3 also reduces the severity of symptoms in mouse models of numerous neurological diseases, including Alzheimer's disease[5,6], frontotemporal lobe dementia[7], neuropathic pain[8], and virus-induced memory impairment[9], and variations in the human C4 gene contributes towards schizophrenia risk[10]. These studies suggest that dysregulation of the complement system plays an important role in synapse loss in pathological states. In the peripheral immune system, the complement system is kept under tight control by a variety of complement inhibitors[11] to prevent runaway activation and damage to self-tissue. However, whether the brain expresses endogenous complement inhibitors to protect synapses against complement-mediated synapse elimination is unknown.

We have previously shown that sushi repeat protein X-linked 2 (SRPX2), a secreted sushi domain protein expressed by neurons, can increase glutamatergic synapse density[12]. Mutations in the human SRPX2 gene are associated with language disorders[13-15], and the SRPX2$^{-/Y}$ mouse displays both decreased thalamocortical synapse densities and abnormalities in ultrasonic vocalization[16]. Sushi domains are also known as complement control protein (CCP) modules, because many known complement inhibitors contain these domains[17]. Many orphan sushi domain proteins are expressed in the mammalian brain and are implicated in neurodevelopmental diseases[18-20], suggesting that they have a role in brain development. However, the molecular mechanism utilized by sushi domain proteins to affect brain development remains unknown.

Here, we provide evidence that SRPX2 is a complement inhibitor which protects synapses against complement-mediated elimination. We show that SRPX2 directly binds to C1q, the initiating component of the classical complement pathway, and inhibits complement activation. In the SRPX2$^{-/Y}$ mouse, complement and microglial activation are increased. In the dorsal lateral geniculate nucleus (dLGN) of the SRPX2$^{-/Y}$ mouse, we observed reduced numbers of retinogeniculate synapses, increased microglia engulfment of synapses, and increased segregation of RGC axons. The C3$^{-/-}$ mouse has the opposite phenotypes, and in the C3$^{-/-}$;SRPX2$^{-/Y}$ double knockout mouse, the C3$^{-/-}$ phenotypes are dominant, indicating that an intact complement system is required for SRPX2's effect on synapses. In the somatosensory (SS) cortex, the SRPX2$^{-/Y}$ mouse shows a decreased density of thalamocortical synapses, while corticocortical and inhibitory synapses are unaffected. We show that the decreased thalamocortical synapse density is due to increased synapse elimination in the SS cortex, and that this phenotype is occluded or reversed in the C3$^{-/-}$;SRPX2$^{-/Y}$ mice. Our findings implicate the sushi domain proteins in the regulation of complement-mediated synapse elimination in the CNS.

Author Manuscript Author Manuscript Author Manuscript Author Manuscript

RESULTS

SRPX2 binds to C1q

To characterize the molecular pathway utilized by SRPX2 to increase synapse density, we sought to identify interactors of SRPX2 by immunoprecipitating (IPing) native SRPX2 complexes from mouse brain. Because our anti-SRPX2 antibodies do not IP well, we made a SRPX2-FLAG knockin (KI) mouse model with CRISPR technology (Extended Data Fig. 1a), and verified that the FLAG epitope is correctly appended at the C-terminus of SRPX2 by sequencing (Extended Data Fig. 1b). In the SRPX2-FLAG-KI mouse, SRPX2-FLAG is expressed under the control of its endogenous promoters and is expressed at its normal levels and locations (Extended Data Fig. 1c), reducing the chances of artefactual binding to other proteins. We have previously shown that tagging SRPX2 at the C-terminus with FLAG does not affect its synaptogenic activity[12]. Using this mouse model, we IPed SRPX2-FLAG from brain lysates using the well-characterized anti-FLAG M2 monoclonal antibody. As sushi domain proteins are known to interact with complement components[17], we blotted the IP for complement components known to be expressed in the CNS[21]. We found that C1q coIPs with SRPX2-FLAG, while C3 does not (Fig. 1a). To ensure the specificity of the coIP, we also performed the IP on WT mice lacking the FLAG epitope, and showed that C1q is not IPed by M2 antibody in WT mice (Fig. 1a). These results indicate that SRPX2 and C1q are present in the same protein complex in the brain.

While both SRPX2 and C1q are present in the same protein complex, SRPX2 could bind directly to C1q, or indirectly through other proteins. To distinguish between these possibilities, we performed coIP experiments with HEK cells cotransfected with C1qa/b/c and SRPX2-FLAG to look for direct interaction. Anti-FLAG M2 beads coIPs C1qa/b/c in the presence of SRPX2-FLAG (Fig. 1b), and does not in the absence of SRPX2-FLAG, indicating the specificity of the coIP. C1q is a hexameric protein complex composed of the three genes C1Qa/b/c, which raises concerns about whether it is able to assemble correctly in a heterologous cell line. However, a previous study has shown that it is possible to generate functional C1q in HEK cells by increasing the dosage of the C1qc gene relative to C1qa and C1qb[22], and we adopted this protocol here. While we were able to coIP SRPX2 and C1q from solubilized HEK cell lysate, we were unable to do so from conditioned HEK cell medium (Fig. 1c), despite the presence of both proteins in the medium. We have also tried directly binding purified C1q to SRPX2-FLAG without success (data not shown). This lack of binding in the fluid phase may be due to the known behavior of C1q to bind some ligands only when immobilized on a solid substrate[23,24]. This would account for our ability to coIP SRPX2 and C1q from HEK cell lysates, which would contain C1q bound to cell membranes, while not being able to do so from HEK conditioned medium or with purified C1q in solution. To test this hypothesis, we performed a dot blot overlay assay, in which we bound increasing amounts of purified C1q, C3b and BSA onto nitrocellulose membranes, and then applied SRPX2-FLAG conditioned medium (Fig. 1d). In this assay, SRPX2-FLAG displays dose-dependent saturable binding to immobilized C1q, but not C3b, again demonstrating direct binding between SRPX2 and C1q.

Author Manuscript Author Manuscript Author Manuscript Author Manuscript

Previous studies have shown an excess of synapses in the dLGN[3] and layer 4 (L4) of the cortex[4] in complement-related gene knockouts. We therefore focused on these regions in our studies. To determine the cell type which expresses SRPX2, we first performed RNAscope *in situ* hybridization for SRPX2 mRNA in the dLGN at P10, and in L4 SS cortex at P60 (Fig. 2a,b and Extended Data Fig. 2a). Consistent with previous studies[14,25] and the Allen Brain Atlas, we found that SRPX2 is expressed primarily in neurons, with SRPX2 mRNA being enriched in NeuN-positive neuronal soma compared to Iba1/GFAP/Olig2-positive microglia/astrocyte/oligodendrocyte soma in both brain regions (Fig. 2b). To determine if SRPX2 protein is colocalized with complement components and synapses *in vivo*, we performed immunohistochemistry (IHC) followed by quantitative cross-correlation analysis. We observed that SRPX2 puncta were most highly correlated with C1q puncta (Fig. 2c,d), with non-colocalized puncta presumably reflecting distribution of secreted SRPX2 in the extracellular space. SRPX2 puncta also show weaker correlations with excitatory presynaptic puncta VGlut1/VGlut2, and no correlation with C3 puncta and inhibitory presynaptic VGAT puncta (Fig. 2d). As an independent assay of synapse localization, we blotted for SRPX2 in synaptosome preparations, and found that both SRPX2 and C1q can be found in the synaptosome fraction (Extended Data Fig. 2b), although both proteins can also be found in the soluble fractions, as is expected for secreted proteins. Taken together, these experiments indicate that SRPX2 binds to C1q in the mouse brain.

SRPX2 inhibits the classical complement pathway

Next, we sought to determine the functional effect of SRPX2 binding to C1q. We first tested the ability of SRPX2 to inhibit complement activation in the CH_{50} total hemolytic complement activity assay, which assesses the functional ability of normal human serum to generate hemolytic terminal complement complexes (TCC). When SRPX2-FLAG is incubated with serum, the generation of TCC is strongly reduced (Fig. 3a). To determine if SRPX2 inhibits complement activation at the C1 step, we further tested the ability of SRPX2 to inhibit cleavage of C2 by C1 *in vitro*. We found that preincubation of purified C1 with SRPX2-FLAG decreases its ability to cleave C2 (Fig. 3b,c), indicating that SRPX2 acts at the level of C1.

To determine whether the loss of SRPX2 *in vivo* leads to complement activation in the brain, we generated the SRPX2 knockout mouse[16], and performed IHC for C1q and C3 on their brain slices. We detected equivalent levels of C1q in P10 dLGN and P60 L4 SS cortex of $SRPX2^{+/Y}$ and $SRPX2^{-/Y}$ mice, but observed large increases in C3 deposition in the $SRPX2^{-/Y}$ mouse in both brain regions (Fig. 3d-g), consistent with SRPX2 blocking complement activation at the C1 step. To exclude the possibility that excess C3 deposition could lead to neurodegeneration, we stained for neurodegeneration markers APP, ATF3, and cleaved caspase 3, and found no detectable levels of these markers (Extended Data Fig. 3a-c). We also assessed microglia for expression of markers associated with homeostatic (P2RY12, TMEM119) or neurodegenerative (ApoE, Clec7a) states[26], and found comparable expression of all microglial markers in $SRPX2^{+/Y}$ and $SRPX2^{-/Y}$ mice (Extended Data Fig. 3d-g). Therefore, despite excess C3 levels, there is no neurodegeneration within the $SRPX2^{-/Y}$ brain. These findings show that SRPX2 acts to inhibit the classical complement pathway in the brain, and in its absence, the complement system is aberrantly activated.

Author Manuscript Author Manuscript Author Manuscript Author Manuscript

SRPX2 deletion reduces numbers of retinogeniculate synapses in the dLGN

The retinogeniculate synapses of the dLGN have previously been shown to undergo developmental complement-mediated synapse elimination in the first month after birth[2]. We then sought to examine if SRPX2 knockout causes functional overpruning of retinogeniculate synapses using an established electrophysiological assay at this synapse[27]. We recorded from dLGN relay neurons of P10 $SRPX2^{+/Y}$ and $SRPX2^{-/Y}$ mice while stimulating the optic tract with increasing stimulation intensities. Minimal stimulation intensities allow the determination of single-fiber input currents, while high stimulation intensities stimulate all intact RGC inputs to the cell. Consistent with fewer retinogeniculate synapses in the $SRPX2^{-/Y}$ mice, we observed a decrease in maximal currents in dLGN neurons (Fig. 4a,b), with a significant reduction in maximal AMPA receptor current (Fig. 4d), as well as a lower median NMDA receptor current, although the latter decrease was not significant (Fig. 4e). Cumulative amplitude histograms of both AMPA receptor and NMDA receptor currents also show a leftward shift for $SRPX2^{-/Y}$ mice, indicating lower currents (Fig. 4c). To estimate the number of retinal inputs synapsing on each dLGN neuron, we calculated the fiber fraction (FF) for each dLGN neuron recorded, defined as the ratio of the single fiber input current to the maximal current[28]. We observed a higher FF in $SRPX2^{-/Y}$ mice (Fig. 4f). Together, these data indicate that P10 dLGN neurons in the $SRPX2^{-/Y}$ mice have fewer retinogeniculate synapses compared to wildtype.

SRPX2 regulates complement-mediated RGC axon segregation in the dLGN

To determine if loss of synapses in the $SRPX2^{-/Y}$ mice requires an intact complement system, we generated mice of two additional genotypes: the $C3^{-/-}$ knockout and the $C3^{-/-}$;$SRPX2^{-/Y}$ double knockout mice. We first performed DAPI/Nissl/myelin staining to verify that major cell layers and axonal tracts are intact in mice of all 4 genotypes (Extended Data Fig. 4). Next, we examined the mice with an anatomical assay which has been extensively used to study retinogeniculate synapse elimination[2,3,29], the developmental segregation of retinal axons in the dLGN. We injected different dye-conjugated anterograde tracers separately into the eyes of P3/P9/P29 mice (Fig. 5a), sectioned their brains 24 hours later, and quantitated the degree of overlap between axons from the ipsilateral and contralateral eyes. At P4 and P10, axons from both eyes show a lower degree of overlap in $SRPX2^{-/Y}$ mice compared to $SRPX2^{+/Y}$ mice (Fig. 5b,c and Fig. 5e,f). We also replicated previous reports that C3 deletion decreases synapse elimination in this system[2,3], and also observed that C3 co-deletion occluded the $SRPX2^{-/Y}$ phenotype at P4 (Fig. 5b,e), and reversed it at P10 (Fig. 5c,f) . However, by P30, both $SRPX2^{+/Y}$ and $SRPX2^{-/Y}$ mice have reached near-maximal axon segregation, and there is no difference between the two genotypes (Fig. 5d,g), although the $C3^{-/-}$ phenotype is still dominant in the $C3^{-/-}$;$SRPX2^{-/Y}$ double knockout mice. These findings show that SRPX2 regulates retinogeniculate synapse elimination transiently during early development, and that this regulation requires C3.

Author Manuscript Author Manuscript Author Manuscript Author Manuscript

SRPX2 deletion increases complement-mediated microglial engulfment of synapses in the dLGN

Complement activation triggers synapse elimination through microglial phagocytosis of excess synapses[3]. To investigate whether increased RGC axon segregation in the dLGN of SRPX2$^{-/Y}$ mice takes place through the complement-microglia pathway, we performed IHC for C3 levels in the dLGN. We found that C3 levels are elevated in the SRPX2$^{-/Y}$ mice at P4 and P10, but has declined to wildtype levels by P30 (Fig. 6a-c). We also assessed the general endocytotic activity of microglia by quantitating the percentage of Iba1-positive microglial volume occupied by CD68-positive lysosomes, and found that lysosome content of microglia in the SRPX2$^{-/Y}$ dLGN were elevated at P4 and P10, but was comparable to wildtype SRPX2$^{+/Y}$ at P30 (Fig. 6d-g) To assess microglial engulfment of RGC axons, we injected tracer into both eyes of mice, and quantitated the amount of tracer within microglial lysosomes[3,28] (Fig. 6h,i and Extended Data Fig. 5). SRPX2$^{-/Y}$ mice had elevated levels of microglial axon engulfment at P4 and P10, whereas the C3$^{-/-}$ and C3$^{-/-}$;SRPX2$^{-/Y}$ mice showed reduced levels of microglial axon engulfment at the same time points (Fig. 6j,k). By P30, all genotypes showed a low level of microglial axon engulfment (Fig. 6l). To directly quantify the number of retinogeniculate synapses in the dLGN, we performed IHC for colocalized VGlut2/PSD95 puncta in the core region of the dLGN[28]. We found that retinogeniculate synapses were reduced in SRPX2$^{-/Y}$ mice at P4 and P10, but were comparable to wildtype mice at P30 (Fig. 6m-o), indicating that the transient increase in C3 deposition and microglial activation in the dLGN resulted in a similarly transient decrease in synapse density which is largely absent by P30. These data indicate that during early development, microglia in the SRPX2$^{-/Y}$ mouse engulf more RGC axons in the dLGN, resulting in lower synapse densities. This phenotype requires the presence of C3, and is consistent with SRPX2 being an upstream inhibitor of the complement system.

SRPX2 inhibits complement activation in L4 SS cortex but not L2/3

We have previously shown that thalamocortical synapses in L4 SS cortex is decreased in the SRPX2$^{-/Y}$ mouse[16]. To investigate whether SRPX2 also inhibits complement and microglial activation in the cortex, we performed IHC for C3, Iba1 and CD68 in P60 L4 SS cortex. As control, we also examined the same markers in L2/3. We found elevated levels of C3 in L4, but not L2/3 (Fig. 7a,b). Similarly, microglia from SRPX2$^{-/Y}$ mice contained higher levels of CD68 lysosomal markers compared to wildtype mice in L4, but not in L2/3 (Fig. 7c,d), indicating layer specificity in complement/microglial activation in SRPX2$^{-/Y}$ mice.

To determine if the layer specificity in C3 deposition and microglia activation extended to synapse density, we performed Golgi staining to visualize dendritic spines in L4 and L2/3 of the SS cortex. In L4, we quantified ascending apical dendrites of L5 pyramidal neurons and descending basal dendrites of L2/3 pyramidal neurons that reside in L4 (Fig. 7e). Thalamic axons have been shown to synapse on both populations of dendrites with classical histological methods[30], modern optogenetic mapping[31], as well as 3D EM reconstruction[32]. We did not directly quantify dendrites of stellate cells in L4 because we had previously found they had variable spine densities depending on their positions within the barrel, which is difficult to discern under Golgi when <1% of neurons are stained[16]. As control, we also quantitated spine density on apical dendrites of L2/3 neurons, which ascend through L2/3

Author Manuscript Author Manuscript Author Manuscript Author Manuscript

and are not innervated by thalamic inputs (Fig. 7f,g). We found that spine densities of L2/3 basal and L5 apical dendrites were decreased in the SRPX2$^{-/Y}$ mice, and that C3 co-deletion normalized the spine densities in the C3$^{-/-}$;SRPX2$^{-/Y}$ mice (Fig. 7h-k), indicating that C3 is also required for the reduction of synapse densities. Spine density on apical dendrites of L2/3 neurons were unchanged in all genotypes (Fig. 7f,g). These data show that SRPX2 deletion causes complement activation, microglial activation, and thalamocortical synapse loss, specifically in L4 SS cortex, and that these phenotypes require C3.

SRPX2 regulates complement-mediated synapse elimination in the SS cortex

To determine if the reduction in spine density in the SS cortex of SRPX2$^{-/Y}$ mice is due to an increase in synapse elimination, we assessed C3 deposition, microglial engulfment of synapses, and synapse density in L4 over time, at P30/P60/P90, a period of time over which developmental synapse elimination has been shown to occur in the cortex[33]. We performed IHC for C3, and found that SRPX2$^{-/Y}$ mice C3 levels were normal at P30, elevated at P60, and has largely declined back to wildtype levels by P90 (Fig. 8a-c). To assess whether elevated C3 levels led to increased microglial engulfment of synapses, we quantitated the amount of VGlut2 within Iba1 and CD68-positive microglial lysosomes, and found that microglial engulfment of VGlut2 synapses in the SRPX2$^{-/Y}$ mice was similarly elevated at P60, but normal at P30 and P90 (Fig. 8d-g and Extended Data Fig. 6). Increased microglial engulfment of synapses is dependent on the presence of C3, and microglial engulfment was reduced at all time points in the C3$^{-/-}$ and C3$^{-/-}$;SRPX2$^{-/Y}$ mice. To assess synapse density over time, we measured the spine density on the basal dendrites of L2/3 pyramidal neurons which ramify in L4, a set of dendrites which has been shown to undergo spine pruning over the age of 1-3 months, with most of the pruning occurring at 2-3 months in wildtype mice[33]. In SRPX2$^{-/Y}$ mice, we observed precocious and increased spine pruning starting at P30 (Fig. 8h,i). Conversely, the C3$^{-/-}$ mice showed nearly no spine pruning from P30 to P90 (Fig. 8h,i), and had significantly more spines than wildtype mice at P90. In the C3$^{-/-}$;SRPX2$^{-/Y}$ mouse, we also observed minimal spine pruning from P30 to P90, indicating that C3 co-deletion occludes the SRPX2 phenotype (Fig. 8h,i). To verify these results independently, we performed IHC for the corticocortical synapse markers VGlut1/PSD95, thalamocortical synapse markers VGlut2/PSD95, and inhibitory synapse markers VGAT/gephyrin. We observed that deletion of C3 did not affect the number of VGlut1/PSD95 synapses at all ages P30/P60/P90, but increased the number of VGlut2/PSD95 and VGAT/gephyrin synapses at P60 and P90 (Fig. 8j-m), suggesting that complement-mediated synapse elimination affects both VGlut2/PSD95 and VGAT/gephyrin synapses in L4 SS cortex. Although we did not see increased spine density at P60 for C3$^{-/-}$mice in the Golgi assay (Fig. 8i), this is probably due to a slightly different time course of synapse elimination when assessing the total VGlut2 synapse population versus a smaller subset of synapses on L2/3 basal dendrites. We also observed that SRPX2 deletion decreased the density of VGlut2 synapses but not VGAT synapses at both P60 and P90 (Fig. 8j-m), indicating that SRPX2 protects VGlut2 synapses specifically. While C3 levels and microglial engulfment of synapses in the SRPX2$^{-/Y}$ mouse has largely declined to wildtype levels by P90, synapse levels were still reduced at P90, suggesting that a transient increase in microglial synapse engulfment in the cortex may lead to circuitry changes that persist past the period of microglial dysfunction. We also observed that in the C3$^{-/-}$;SRPX2$^{-/Y}$ mouse, the C3$^{-/-}$

Author Manuscript Author Manuscript Author Manuscript Author Manuscript

phenotypes were always dominant over the SRPX2$^{-/Y}$ phenotypes, indicating that C3 is required for the SRPX2 phenotypes. Taken together, these results show that SRPX2 decreases synapse elimination through inhibiting the complement system in multiple regions of the brain.

DISCUSSION

We have identified SRPX2 as a novel complement inhibitor that regulates complement-mediated synapse elimination in both the dLGN and L4 SS cortex. In the dLGN, SRPX2 regulates complement activation and microglial engulfment of RGC axons, thereby transiently affecting synapse elimination during development. In L4 SS cortex, SRPX2 regulates the elimination of thalamocortical synapses through the same pathway. Thus, this work provides a molecular mechanism for the spatial and temporal control of complement activity in the brain, restricting complement-mediated synapse elimination to specific synapse populations and time periods during brain development.

SRPX2 was initially identified in a high throughput screen in cultured cortical neurons on the basis of its ability to increase excitatory synapse density when overexpressed[12], but it was unclear whether SRPX2 exerts its synaptogenic activity by increasing the rate of synapse formation, or decreasing the rate of synapse elimination. Our results suggest that SRPX2 regulates synapse elimination rather than formation, for two reasons. Firstly, in the SS cortex, spine pruning starts from the same baseline at P30 for all genotypes (Fig. 8i), suggesting similar rates of synapse formation in all genotypes. Secondly, our genetic epistasis experiments suggest that SRPX2 regulates the complement-microglia pathway, a pathway known to be involved in synapse elimination. If SRPX2 affects synapse formation and C3 affects synapse elimination, with both operating in separate pathways, the linear summation of their phenotypes should result in the C3$^{-/-}$;SRPX2$^{-/Y}$ having a phenotype that is intermediate between the SRPX2$^{-/Y}$ and C3$^{-/-}$ phenotypes. However, in our study, the C3$^{-/-}$ phenotype is always dominant in the C3$^{-/-}$;SRPX2$^{-/Y}$ mouse. In combination with our molecular characterization of the SRPX2-C1q interaction, the most parsimonious explanation for our observations is that SRPX2 is upstream of C3 in the same molecular pathway which affects synapse elimination.

Complement-mediated synapse elimination plays an important role in brain development and neurological diseases. However, whether neurons express endogenous complement inhibitors to protect synapses against complement-dependent pruning was previously unknown. Previous studies have identified several complement regulators in the brain, including CSMD1[34,35] and SUSD4[23], but whether they are involved in synapse elimination is unclear. The mouse retinogeniculate system is a well-studied model system for synapse elimination during development, and previous work has shown that multiple genes regulate the timing and extent of axon segregation in the LGN[36]. Intriguingly, a large number of these genes are also associated with the immune system, including the complement system[2,3], the neuronal pentraxins (NPs)[37], major histocompatibility class I (MHCI) family members[38,39], TGF-β[29], and CD47-SIRPα[28]. Two of these genes are known to interact with the complement-microglia pathway: TGF-β secretion from astrocytes has been shown to control C1q expression at the transcriptional level in RGCs[29]; and CD47 binds to SIRPα on

Author Manuscript Author Manuscript Author Manuscript Author Manuscript

microglia to decrease phagocytosis at a step downstream of the complement system[28]. Here, we show that SRPX2 is a novel complement inhibitor that acts by binding to C1q and inhibiting its cleavage of C2, thereby reducing the downstream deposition of C3b onto membranes and microglial phagocytosis of synapses. While we cannot exclude the possibility that SRPX2 may regulate other biological processes through other binding partners[40,41], its regulation of synapse elimination in the LGN is C3-dependent. Our findings suggest that other immune-associated genes implicated in synapse refinement in the LGN may also act by interacting with the complement system.

In the human cortex, it has long been known that net synapse elimination occurs during adolescence[42], generally starting in the primary sensory cortices and proceeding to higher cortical areas[43], over an extended time frame that may span decades[44]. This phenomenon is conserved across many mammalian species, including in primates and rodents[33,45,46], and is maximal in mid-adolescence, at 2-3 month in rodents[33]. Early studies to determine the role of complement in cortical synapse elimination utilized C1q knockout mice at around P30, and observed increases in spine densities of L5 neurons in the sensorimotor cortex, and increased responses to uncaged glutamate in L4 and L5[4,47]. However, later studies in the cortex using sensory lesion models have given conflicting results. A study using the whisker-trimming model in CR3-deficient mice found that CR3 is dispensable for lesion-induced loss of thalamocortical inputs to the SS cortex in P4-P10 mice, whereas CX3CL1-CX3CR1 signaling is required[48]. Another study examining ocular dominance plasticity (ODP) in V1 cortex of C1q knockout mice showed that basal development of spines on L2/3 neurons were unchanged from P10-P30, and C1q is dispensable for ODP[49]. Here, we observed an excess of VGAT/gephyrin and VGlut2/PSD95 synapses in L4 SS cortex of the P60-P90 C3 knockout mouse, whereas VGlut1/PSD95 synapses were unchanged, suggesting that the complement system only mediates elimination of specific populations of synapses in the cortex. Several factors may account for the divergence of results in the literature, including the use of developmental versus lesion-induced synapse elimination models, the time points utilized, and the specific brain region and set of synapses examined. In addition, our study suggests that a transient increase in complement-mediated synapse elimination in the SS cortex can lead to a long-lasting decrease in synapse density, although future work is required to determine the exact duration and extent of cortical synapse losses induced by deletion of SRPX2. Lastly, all studies of complement-mediated synapse elimination to date have utilized constitutive knockout mice, in which synapse density changes observed in a particular brain region may be due to changes in activity or connectivity in afferent brain regions. Therefore, conclusive evidence of complement-mediated synapse elimination in the cortex and LGN may require the use of cell-specific knockouts.

Complement-mediated synapse losses have been shown to occur in many neurological diseases[5-7,10]. An important question in disease pathogenesis is why pathological complement activation often leads to the loss of particular subsets of synapses[7,9], despite the pathogenic insult causing complement activation throughout the brain region. Our findings suggest that different complement inhibitors may protect different sets of synapses, and that changes in the levels of complement inhibitors may account for the differential vulnerability of brain circuits to aberrant complement activation. Furthermore, drugs that alter levels of complement inhibitors may represent a new therapeutic approach for the treatment of

Author Manuscript Author Manuscript Author Manuscript Author Manuscript

complement-associated neurological diseases, with the potential for targeted therapeutic effects at specific sets of synapses. At the level of the human population, the inherited set of common variants in complement and complement-regulating genes in an individual, dubbed the “complotype”, has been shown to contribute to individual susceptibility to immunological diseases[50], and may well contribute towards the polygenic risk of psychiatric diseases, as has been shown in the case of schizophrenia[10]. Further work is required to reveal the full repertoire of complement inhibitors in the brain, which will provide broad insights into the pathophysiological processes underlying many neurodevelopmental and neurodegenerative diseases, and may represent a novel point of intervention for their therapy.

METHODS

Animals.

The SRPX2$^{FLAG/Y}$ mouse was generated with CRISPR/Cas9 on the C57BL/6J genetic background. We designed an sgRNA targeting SRPX2 exon 12 near the stop codon, as well as corresponding repair oligonucleotides containing the FLAG epitope and stop codon (Fig. 1A), thereby adding a FLAG epitope to the C-terminus of SRPX2. To facilitate the detection of the inserted oligo, we also introduced a SpeI restriction site into the repair oligo (Fig. 1B). The sgRNA, Cas9 mRNA, and repair oligo into the zygotes of C57BL/6J mice (Jackson stock 000664), which were transferred into pseudo-pregnant female mice. We obtained 34 founder mice from the injection. Each founder mice was PCR screened with primers surrounding the expected site of editing, and the PCR fragments were cut with the SpeI enzyme to detect the presence or absence of the inserted oligo. We recovered 19 positive mice out of 34 mice from this screen. Subsequent subcloning and sequencing of the PCR products from these mice revealed that the vast majority of the mice contained SRPX2-FLAG alleles of the correct sequence (Fig. 1B), and immunoblotting revealed the presence of the FLAG epitope in the brain of the knockin mice.

The SRPX2$^{-/Y}$ mouse was generated as described previously[16], and maintained on a C57BL/6J background. The C3$^{-/-}$ mouse was obtained from Jackson (stock 003641), and was backcrossed to C57BL/6J for 5 generations before use in experiments. The C3$^{-/-}$;SRPX2$^{-/Y}$ mice were generated by crossing above two lines. Experiments were performed with male littermates from heterozygous breeding pairs. We used only male WT and KO mice because SRPX2 is an X-linked gene, and it is not possible to generate female WT and KO pups in the same litter, and random X-inactivation render heterozygous mice unsuitable for experiments. Mice were maintained in the UTHSCSA animal facility under a 12 hour light:dark cycle with ad libitum access to food and water. Mice of different genotypes were processed in random order for all experiments. All animal work was approved by the UTHSCA Institutional Animal Care and Use Committee (IACUC).

Cell culture.

HEK293T cells (ATCC Cat. no. CRL-3216) were cultured in DMEM (Gibco, Cat no. 1961585) supplemented with 10% fetal bovine serum (Invitrogen, Cat no. 10437028), 2mM L-Glutamine (Invitrogen, Cat. no. 25030-081), and Penicillin-Streptomycin solution (5

Author Manuscript Author Manuscript Author Manuscript Author Manuscript

U/mL, 5 μg/mL) (Invitrogen, Cat. no. 15070063). HEK293T cells were transfected using Lipofectamine 2000 (Invitrogen, Cat. no.1854317) according to the manufacturer's instructions.

Plasmids.

SRPX2-FLAG-pCAG was generated by PCR-amplifying SRPX2 (NM_026838) from murine brain cDNA, and subcloning the PCR fragment with a C-terminal FLAG tag into a pCAG vector between the NotI and EcoRV sites. HA-C1qa, HA-C1qb, and HA-C1qc plasmids were generated by PCR-amplifying murine C1qa (NM_007572), C1qb (NM_009777), and C1qc (NM_007574) from murine brain cDNA, and cloning the fragments into a pCAG vector between the EcoRI and XhoI sites, inserting an N-terminal HA (YPYDVPDYA) epitope tag after the signal peptide.

Co-immunoprecipitation from brain lysates.

Adult 2 month old $SRPX2^{+/Y}$ and $SRPX2^{FLAG/Y}$ mice were anesthetized and perfused with phosphate buffer saline (PBS). Brains were dissected and homogenized in lysis buffer containing 50 mM Tris, pH 7.5, 1% Triton X-100, 150 mM NaCl, 10% glycerol, and 2 mM PMSF using a Glas-Col homogenizer at 10 mL lysis buffer per gram wet weight. Brain homogenates were incubated at 4 °C for 30 min and then centrifuged at 1000 x g for 10 min, and 21,000 x g for 30 min at 4 °C. For co-immunoprecipitation, the supernatant was further incubated with anti-FLAG M2 magnetic beads (Sigma-Aldrich, Cat. no. M8823-1ML) for 3 hours at 4 °C. Magnetic beads were extensively washed with lysis buffer and TBS (50 mM Tris HCl, 150 mM NaCl, pH 7.4). Protein complexes were eluted with 100 μL of 3X FLAG peptide (200 ng/μL) according to the manufacturer's protocol (Sigma-Aldrich), and the eluates were blotted with anti-FLAG M2-peroxidase (HRP) (Sigma-Aldrich, Cat. no. A8592-0.2mg), anti-C1Q (Abcam, Cat no. ab182451), and anti-C3 (MP Biomedicals, Cat. no. 0855730) antibodies. For checking endogenous SRPX2 expression in the $SRPX2^{FLAG/Y}$ knock-in mouse, the brain was dissected into whole brain (WB), cortex (CX), and mid-brain (MD) before homogenization, and the lysates were blotted with anti-SRPX2 (Creative Biolabs, Cat. no. CBMAB-S1587-CQ) and anti-GAPDH (Novus Biologicals, Cat. no. NB600-502).

Co-immunoprecipitation from HEK293T cells.

HEK293T cells in Opti-MEM medium were cotransfected with the HA-C1qa and HA-C1qb plasmids using Lipofectamine 2000 (Invitrogen, Cat. no.1854317) according to the manufacturer's protocol for 2 hours. These cells were then similarly cotransfected with HA-C1qc and SRPX2-FLAG plasmids for 4 hours as described in a previous report[50]. HEK cells were then left in new Opti-MEM for 48 hours, and then harvested and spun at 5000 g for 10 min to separate cells from medium. The cell pellet was lysed in The cell medium was diluted with an equal volume of 2x lysis buffer (100 mM Tris, pH 7.5, 2% Triton X-100, 300 mM NaCl, 2 mM EDTA, 10 mM PMSF and 2 x cOmplete Ultra). The cell pellet was lysed in 1x lysis buffer (50 mM Tris, pH 7.5, 1% Triton X-100, 150 mM NaCl, 1 mM EDTA, 1 mM PMSF and 1x cOmplete Ultra) for 30 min at RT, and then spun down at 5000 g for 10 min. The supernatant/cell medium was incubated with anti-FLAG M2 magnetic beads (Sigma-Aldrich, Cat. no. M8823-1ML) overnight at 4 °C. Magnetic beads were extensively washed

Author Manuscript Author Manuscript Author Manuscript Author Manuscript

with lysis buffer and TBS (50 mM Tris HCl, 150 mM NaCl, pH 7.4). Protein complexes were eluted with 100 μL of 0.1 M citrate buffer (pH 3.1) according to the manufacturer's protocol (Sigma-Aldrich) and then neutralized. The immunoprecipitation of proteins was detected with monoclonal anti-FLAG M2 (Sigma-Aldrich, Cat no. F1804), and rabbit anti-HA (QED Bioscience, Cat. no. 18850) antibodies.

Western blot.

Brain lysates or cell lysates were mixed with 4 x NuPAGE LDS sample buffer (ThermoFisher Scientific, Cat. no. NP0008), boiled for 10 min at 95 °C and centrifuged at 21,000x g for 10 min. Total protein concentrations was determined and equal amounts of proteins were loaded for SDS-PAGE and blotted on PVDF membrane. After blocking in 5% milk in Tris-buffered saline/Tween (TBS-T, 20 mM Tris, 150 mM NaCl, pH 7.4, 0.1% Tween-20), membranes were incubated with primary antibodies overnight at 4 °C, then washed and incubated with the corresponding HRP-conjugated secondary antibodies for 2 h at room temperature. Quantification of blots were performed using the ImageJ software.

Dot blot.

Complement C1Q, C3b (Complement Technology, Cat. no. A099, Lot 40, and A114, Lot 23a) and BSA (Sigma-Aldrich, Cat. no. A9647-100G) were diluted in TBS and transferred onto pre-rinsed nitrocellulose membranes with a Bio-Dot microfiltration apparatus. The membrane was blocked with 5% milk for 1 hour, incubated with conditioned HEK cell media for 2 hours, and then detected with anti-FLAG M2 monoclonal antibody (Sigma-Aldrich, Cat. no. F1804).

CH50 assay.

HEK293T cells were transfected with SRPX2-FLAG-pCAG or pCAG empty, maintained in the Opti-MEM medium (Gibco, Cat no. 1929947) for 3 days, lysed in cell lysis buffer (50 mM Tris, 0.1% Triton X-100, 150 mM NaCl, 1 mM EDTA, and 1x cOmplete Ultra), then concentrated with Amico Ultra 0.5 mL centrifugal filter (MilliporeSigma, Cat. no. UFC503008, 30,000 NMWL). The retentates were used as test samples with the MicroVue CH50 Eq EIA kit (Quidel, Cat. no. A018). Briefly, 5 μL of the test samples were mixed with 5 μL of normal human serum and incubated at 37 °C for 30 min. Aggregated IgG activator solution was then added to each sample, and complement activation was allowed to proceed for 1 hour at 37 °C. To assess the degree of complement activation, test samples are diluted 1:200 into diluent solution, and 100 μL of the diluted samples are pipetted into microwell plates, which is then covered with an adhesive film and incubated at RT for 1 hour with shaking to allow deposition of terminal complement complexes (TCC). TCC were then detected with an ELISA assay according to manufacturer's instructions, and the plate is read at OD 450 nm with a plate spectrophotometer. Assay results were expressed in CH50 unit equivalents per milliliter (CH50 U Eq/mL) by reference to the kit standard curve.

C2 cleavage assay.

The assay was performed as previously described[51], with minor modifications. HEK293T cells were transfected with SRPX2-FLAG-CAG or empty vector, maintained in the Opti-

Author Manuscript Author Manuscript Author Manuscript Author Manuscript

MEM medium (Gibco, Cat. no. 1929947) for 2 days, and then lysed in cell lysis buffer (50 mM Tris, 1% Triton X-100, 150 mM NaCl, 1 mM EDTA, and 1x cOmplete Ultra). After a brief spin at 5000 x g for 10 min, the supernatant was transferred to anti-FLAG M2 magnetic beads (Sigma-Aldrich, Cat. no. M8823-1ML) and incubated overnight at 4 °C. Beads were then extensively washed with lysis buffer and GVB++ buffer (Complement Technology B102). Protein complexes were eluted with 100 μL of 3X FLAG peptide (200 ng/μL in GVB ++ buffer) according to the manufacturer's protocol (Sigma-Aldrich). For the C2 cleavage assay, in a total volume of 100 μL, 60 μL of each eluent was pre-incubated with 0.1 μg/mL of C1 (Complement Technology, Cat. no. A098) for 30 min, and then 2.5 μg/mL of C2 (Complement Technology, Cat. no. A112) was added. The cleavage reaction was allowed to proceed for 1 hour at 37 °C. Recombinant human C1 inhibitor (C1-INH, Tonbo Biosciences, Cat. no. 21-7138-U050) was used as a positive control. Finally, the reaction samples were separated by reducing 10% SDS-PAGE gel, transferred to a PVDF membrane, and detected with goat anti-human C2 primary antibody (Complement Technology, Cat. no. A212) followed by donkey anti-goat IgG secondary antibody (Thermo Fisher, Cat. no. A-21447). To estimate extent of C2 cleavage inhibition, we quantified the ratio of cleaved C2 fragments (C2a and C2b bands) to the total C2 content (C2, C2a and C2b bands). The intensity of each band was analyzed by ImageJ software.

Synaptosome preparation.

Synaptosomes were prepared using the sucrose gradient centrifugation method. Briefly, adult 2 month old mice were killed with CO_2 and their brains were rapidly removed and homogenized with a glass-Teflon homogenizer in an ice-cold homogenization buffer (0.32 M sucrose, 5 mM HEPES, pH 7.5, 0.1 mM $CaCl_2$ and freshly prepared 1 x cOmplete Ultra). The homogenates (H) were centrifuged at 1,000 x g for 10 min at 4 °C to remove the nuclear fraction pellet (P1). The supernatant (S1) was further centrifuged at 21,000 x g for 30 min at 4 °C to generate supernatant (S2) and pellet (P2) fractions. The P2 pellet was homogenized with 10 volumes of ice-cold homogenization buffer and carefully loaded onto a sucrose gradient solution (0.8 M, 1.0 M and 1.2 M sucrose; all with 5 mM HEPES, pH 7.5, 0.1 mM $CaCl_2$ and freshly prepared 1 x cOmplete Ultra). The solution was ultracentrifuged at 50,000 rpm with a rotor SW-55i for 2 h at 4 °C. The synaptosomal fraction was collected from the interface between the 1.0 M and 1.2 M sucrose layers and diluted with 5 volumes of 0.1 mM $CaCl_2$ and further centrifuged at 21,000 x g for 30 min at 4 °C to obtain the pellet. The resulting pellet (Syn) was resuspended in 50 mM Tris, pH 7.5, 1% Triton X-100, and fresh 1 x cOmplete Ultra. All the fractions H, S1, P1, S2, P2, and Syn were stored at −20 °C before western blot analysis. The proteins were blotted with goat anti-C3 (MP Biomedicals, Cat. no. 0855730), mouse IgG1 anti-PSD95 (Synaptic Systems, Cat. no. 24-011), mouse IgG2b anti-SRPX2 (Creative Biolabs, Cat. no. CBMAB-S1587-CQ), and rabbit anti-C1Q (Abcam, Cat. no. ab182451).

RNAscope *in situ* hybridization (ISH) combined with immunohistochemistry (IHC).

To combine RNAscope mRNA detection with antibody-based IHC, two different tissue preparations were used depending on the antibody utilized: fresh frozen tissue was used to detect SRPX2 mRNA and neuronal marker NeuN and oligodendrocyte marker Olig2, and paraformaldehyde (PFA)-fixed tissue was used to detect SRPX2 mRNA and microglia

Author Manuscript Author Manuscript Author Manuscript Author Manuscript

marker Iba1 and astrocyte marker GFAP. For fresh frozen tissue preparation, mouse brains were rapidly dissected and flash frozen with isopentane and dry ice. Twenty μm sections were cut on a cryostat and mounted on Superfrost Plus slides (ThermoFisher Scientific, 4951PLUS-001) and stored at −80 °C. Fresh frozen tissue slides were pre-fixed in 4% PFA at 4 °C for 30 min, then dehydrated slides in serial dilutions of ethanol. For fixed tissue, mice were perfused with PBS, followed by 4% PFA, and post-fixed in 4% PFA for overnight. The post-fixed brains were washed with PBS briefly and cryoprotected in 30% sucrose. Twenty μm sections were cut on a microtome (Leica), floated in water onto Superfrost Plus slides, and air dried overnight at room temperature (RT). ISH was performed on both tissue preparations according to the manufacturer's instruction (ACDBio RNAscope® 2.5 HD Reagent Kit-RED, Cat. no. 322350) with slight modifications. Briefly, tissues were pretreated with hydrogen peroxide for 10 min at RT and Protease Plus for 30 min at RT followed by a wash in PBS. SRPX2 probe (RNAscope® probe Mm-SRPX2, Cat. no. 802711) was added and hybridized in situ at 40 °C for 2 h. Subsequent amplification steps were performed according to the manufacturer's instruction. Due to the low abundance of SRPX2, we extended the AMP 5 incubation time to 45 min. After the chromogen development step, the slides were washed with PBS and PBST (1x PBS containing 0.25% Triton X-100) twice separately. Sections were blocked in PBST containing 2% normal goat serum for 1 h at RT. Primary antibodies of cell-specific marker NeuN (EMD Millipore, Cat. no. ABN91, 1:500), Iba1 (Wako Chemicals, Cat. no. 019-19741, 1:500), GFAP (EMD Millipore, Cat. no. AB5541, 1:500) and Olig2 (Abcam, Cat. no. ab109186, 1:500) were prepared in PBST containing 2% normal goat serum and added on slides. Slides were incubated for overnight at 4 °C and washed with PBST three times. Slides were incubated with secondary antibodies and DAPI prepared in PBST containing 2% normal goat serum for 1 h at RT. After washing with PBST and PBS three times each, slides were cover-slipped with Fluoromount-G (Southern Biotech). Images were acquired with a Zeiss AxioObserver inverted microscope (Zeiss Objective Plan-Apochromat 63x/1.4 Oil) with a Zeiss Apotome.2 module. All images were acquired in 63x magnification and analyzed using Image J (NIH). Each DAPI nucleus is first assigned a cell type based on colocalized markers, and the number of SRPX2 mRNA puncta within the nucleus were then counted.

LGN slice preparation.

Parasagittal brain slices were collected from P10 $SRPX2^{+/Y}$ and $SRPX2^{-/Y}$ mice. Mice were decapitated and brains were rapidly removed and placed in ice cold low calcium artificial cerebrospinal fluid (aCSF) containing (in mM): NaCl, 125; KCl, 2.5; NaH_2PO_4, 1.25; glucose, 25; $NaHCO_3$, 25; $MgCl_2$, 3; and $CaCl_2$, 0.1; ascorbic acid, 0.4; myoinositol, 3; and Na-pyruvate, 2; pH 7.3–7.4 when bubbled with carbogen (95% O_2/5% CO_2), and 310–320 mOsmol/L. Brains were sliced according to a modified protocol of Turner and Salt[52]. In order to maintain the connection between the optic tract and the LGN, 2 slices were made on each side of midline 3-5 degrees to the sagittal plane and 10-25 degrees out in the medio-lateral plane. Each brain half was then glued medial side down onto the cutting stage of a Vibratome (VT1200S, Leica). The sections were then submerged into the above-mentioned solution and cut at 250 μm. Typically, only one slice per hemisphere contained the optic tract and dLGN. Slices incubated for 30 minutes in normal aCSF bubbled with carbogen at 35°C,

Author Manuscript Author Manuscript Author Manuscript Author Manuscript

and thereafter at room temperature. Normal aCSF was the same as low calcium (slicing) aCSF, but with 1 mM $MgCl_2$ and 2 mM $CaCl_2$.

LGN electrophysiological recordings.

Whole-cell voltage-clamp recordings of dLGN neuron were performed using an EPC-10 amplifier (HEKA Elektronik) controlled by Patchmaster software. Recordings were carried out using a cesium methanesulfonate pipette solution contained (in mM): 100 $CsCH_3SO_3$, 20 KCl, 7 Na_2-phosphocreatine, 10 HEPES, 4 Mg-ATP, 0.3 GTP, and 10 EGTA, pH adjusted to 7.3 with KOH. The holding potential was −60 mV for AMPAR-mediated current and +40 mV for NMDAR-mediated current recordings in the voltage-clamp mode. Pipettes were pulled using an electrode puller (Model P-1000, Sutter Instruments) to open tip resistances of 4−5 MΩ. dLGN neurons and optic tract were identified based on neuronal tracer Dil (AAT Bioquest, Cat no. 22102, 2% w/v in DMSO) injected into the retina at P9[27]. A bipolar electrode (Frederic Haer, Bowdoinham, ME) was placed in the optic tract then neurons in the dLGN were recorded. An Iso-Flex stimulator driven by a Master 10 pulse (<10 V constant voltage) was used. Data were analyzed offline and displayed with Igor Pro (Wavemetrics, Lake Oswego, OR).

Labeling of retinogeniculate afferents.

Mouse pups (P3 or P9) were anesthetized by placing them in a glove and briefly immersing them in crushed ice and water for 5-7 min. Adult mice (P29) were anesthesized with Avertin (0.025 mL/g). During the surgery, the hypothermic pups and anesthesized mice were placed on an ice pack (3-4 °C). Pups and mice received intravitreal injections of cholera toxin-β subunit (CTβ) conjugated to Alexa 488 dye (ThermoFisher Scientific, Cat no. C22841, 0.5% in Dulbecco's phosphate buffered saline) into the left eye and cholera toxin-β subunit (CTβ) conjugated to Alexa 555 dye (ThermoFisher Scientific, Cat no. C22843, 0.5% in Dulbecco's phosphate buffered saline) into the right eye (0.5 μL per eye for P3 pups, 1 μL for P9 pups and P29 mice). After the surgery, pups were placed in a slide warmer (Thermo Fisher scientific, Waltham, Massachusetts) at 33°C for at least 1 hour. After 24 hours, pups were transcardially perfused with PBS, then with 4% paraformaldehyde (PFA). Brains were postfixed in 4% PFA for overnight, cryoprotected in 30% sucrose, and then sectioned coronally at 40 μm, mounted on Superfrost Plus slides (Thermo Fisher Scientific, Waltham, Massachusetts), and coverslipped with Fluoromount-G (SouthernBiotech, Birmingham, AL).

LGN axon segregation analysis.

Images were acquired with a Zeiss AxioObserver inverted microscope with a EC Plan-Neofluar 20x/0.5 objective. All images were collected, tiled, and quantified "blind", with the same gain and exposure for each label. The five sections that contained the largest ipsilateral projection, corresponding to the central fifth of the LGN area were selected. All analyses were performed on these sections with an Alexa 488-labeled contralateral/Alexa 555-labeled ipsilateral projection. Raw images of dLGN were imported to Image J and cropped to exclude the vLGN and IGL, then the degree of left and right eye axon overlap was quantified using the previously described multi-threshold protocol[53,54].

Author Manuscript Author Manuscript Author Manuscript Author Manuscript

Immunohistochemistry.

Mice were deeply anesthetized with Avertin (0.5 mg/g) then transcardially perfused with ice-cold PBS and 4% paraformaldehyde (PFA). Brains were immediately removed and post-fixed for 2 hr at 4°C, then cryoprotected in 30% sucrose in PBS for 48-72 hours. Brains were sectioned with a sliding-freezing microtome (Leica) at 20-25 μm (for colocalization analysis, neurodegeneration and microglial markers) or 40 μm (for microglia engulfment and activation staining). Free-floating sections were washed 3x in PBS with 0.2% TX-100 (PBT) then blocked overnight at 4°C in 10% normal donkey/goat serum (Jackson Immunoresearch) in PBT. Slices were incubated with primary antibody overnight at 4°C, washed 4x in PBT, then incubated with secondary antibodies for 2 hr at room temperature. Sections were washed 3x in PBT, 3x in PBS, floated onto glass slides and cover-slipped withed Fluoromount-G (Southern Biotech). The following primary antibodies were used: mouse IgG2b anti-SRPX2 (Creative Biolabs, Cat. no. CBMAB-S1587-CQ, 1: 1500), rabbit anti-C1q (Abcam, ab182451 1:1000), goat anti-rat C3 (MP Bio, 0855730 1:1000), guinea pig anti-VGlut1 (Synaptic Systems, 135-304, 1:2500), guinea pig anti-VGlut2 (Synaptic Systems, 135-404, 1:2500), rabbit anti-Iba1 (Wako Chemicals, 019-19741 1:1000), rat anti-CD68 (Bio-Rad, MCA1957, 1:1000), guinea pig anti-VGat (Synaptic Systems, 131-004, 1:500), mouse IgG1 anti-gephyrin (Synaptic Systems, 147-021,1:500), and mouse IgG1 anti-PSD95 (Synaptic Systems, 124-011, 1:500), rabbit anti-APP (Thermo Fisher Scientific, Cat. no. 51-2700, 1: 1000), rabbit anti-ATF3 (Sigma-Aldrich, Cat. no. HPA001562, 1: 1000), rabbit anti-cleaved caspase 3 (Cell signaling technology, Cat. no. 9661T, 1: 1000), rabbit anti-P2RY12 (Anaspec, Cat. no. AS-55043A, 1: 1000), rat anti-Clec7a (InvivoGen, Cat. no. mabg-mdect, 1: 1000), rabbit anti-TMEM119 (Abcam, Cat. no. ab209064, 1: 1000), goat anti-Apolipoprotein E (EMD Millipore, Cat. no. AB947, 1: 1000), chicken anti-myelin (EMD Millipore, Cat. no. AB9348, 1: 1000), Nissl (ThermoFisher Scientific, Cat. no. B34650, 1: 1000) and DAPI (ThermoFisher Scientific, Cat. no. D1306, 1:300). All secondary antibodies were used at a concentration of 1:500. Secondary antibodies include: goat anti-rabbit Alexa 488 (Thermo Fisher, A-11034), donkey anti-goat Alexa 555 (Thermo Fisher, A-21432), Cy5 AffiniPure donkey anti-guinea pig (Jackson, 706-105-148), Cy5 AffiniPure donkey anti-goat (Jackson, Cat. no. 705-175-147), Cy3 AffiniPure donkey anti-rat (Jackson, 712-165-153), donkey anti-chicken IgY Alexa 488 (Jackson, 703-545-155) and goat anti-mouse IgG1 Alexa 488 (Thermo Fisher, A-21121), goat anti-mouse IgG2b Alexa 555(Fisher scientific, Cat. no. A21147), goat anti-rabbit Alexa 555 (Thermo Fisher, Cat. no. B40923), Cy3 AffiniPure donkey anti-rabbit (Jackson, Cat. no. 711-165-152). All sections were counterstained with DAPI (Thermo Fisher, D1306, 1:300). For cell layer and axonal tracts visualization, BrainStain™ Imaging Kit (Invitrogen, Cat. no B34650) was used following the manufacturer's protocol for Nissl, Fluoromyelin and DAPI staining.

Colocalization, complement deposition & synapse density analysis.

Images were acquired with an Olympus FV-1000 confocal microscope with a Plan Apo 60x 1.3 NA oil-immersion objective, and a Zeiss AxioObserver inverted microscope (Zeiss Objective Plan-Apochromat 63x/1.4 Oil) equipped with a Zeiss Apotome.2 module with the Zeiss Plan-Apochromat 63x/1.4 oil objective. Identical imaging parameters were used for all genotypes under comparison. To colocalize SRPX2 with C1q, C3, VGlut1, VGlut2, and VGAT, determine C1q and C3 deposits, and measure synapse density, we used ImageJ

Author Manuscript Author Manuscript Author Manuscript Author Manuscript

(NIH) for image processing. Individual channels were first Z-projected with summation over a depth of 2 μm and background-subtracted (10px rolling ball radius), followed by a 1px median filter. Threshold channels were empirically determined and then applied consistently to each channel for all subjects. For colocalization analysis, we used the Van Steensel cross-correlation analysis method[55,56] as implemented by the JaCOP ImageJ plugin[57]. For each pair of red and green channels, a cross-correlation function (CCF) was calculated as the green channel was moved with respect to the red channel over a total pixel shift of $\delta = \pm 20$. For quantifying C1q and C3 deposits, the Analyze Particles tool within Image-J was used to quantify the number of individual C1q & C3 puncta. For synapse density, colocalized puncta were determined by using the image calculator tool to multiply the individual pre & post-synaptic channels, and the resulting image was then quantified with the Analyze Particles tool. To identify the dLGN core for analysis of synapse density, DAPI and VGlut2 staining were used to identify the cytoarchitectural borders of the dLGN in coronal slices containing the anterior and middle portions of the dLGN. Shell and core regions were determined based on the width across the dLGN. From the lateral border (close to optic tract, set at 0% width) to the medial border (set at 100% width), the dLGN shell was defined as the region spanning 0%-30% (closest to optic tract and lateral border) of the width across the LGN, and the core region was defined as the region spanning 40%-100% (closest to the medial border) of the width[58].

Microglial engulfment assays and CD68 occupancy.

CTB engulfment in P10 mice and CD68 occupancy within microglia in P60 mice were quantified using Imaris Reconstruction Software (version 9.2, Bitplane, Concord MA), using methods previously described[59]. Reconstructions were performed on high-resolution confocal images of Iba1+ cells with CTB traces or CD68 staining, captured using Plan Apo 60x 1.3 NA oil-immersion objective with a 2.5 zoom to capture a single cell. Using the image processing tool in Imaris, background subtraction was performed on channels containing CTB or CD68 (0.7 μm filter), followed by a Gaussian filter applied to the channel containing Iba1. Iba1-positive cells were surface rendered with 0.1 μm smoothing. Disconnected processes were merged with the cell body to create a single surface. A mask was applied to the surface rendered microglia for the channel containing CD68 to isolate the CD68 signal only within the microglia for surface rendering (0.1 μm smoothing). The volume of the reconstructed surfaces for Iba1 and CD68 were recorded, and the percent of CD68 occupancy within microglia was calculated using the formula: *volume of CD68/ volume of Iba1+ve cell.* For CTB engulfment and VGlut2 engulfment assays, a mask was applied to the surfaced rendered CD68 within microglia for either the CTB or VGlut2 channels to reveal only the CTB or VGlut2 signal within microglial lysosomes. The isolated CTB or VGlut2 channels were surfaced rendered (0.1 μm smoothing) to record the volume. The % engulfment of CTB or VGlut2 within microglial lysosomes was calculated using the formula: *volume of engulfed material found in lysosome/volume of Iba1+ve cell*.

Golgi staining.

Unfixed brains of 1, 2, and 3 month old male mice were processed for Golgi staining using the FD Rapid Golgi Stain Kit (FD Neurotechnologies, Columbia, MD). Immediately following extraction, brains were briefly rinsed in PBS then placed in kit solution A+B for

Author Manuscript Author Manuscript Author Manuscript Author Manuscript

14 days, with gentle rocking and protected from light. Tissue was subsequently transferred to solution C for three consecutive 24 hr periods, while gently rocking. Tissue was then flash frozen with dry ice & isopentane, then sectioned at 200 μm on a Lecia sliding-freezing microtome. Sections were mounted onto gelatin-coated slides and carefully dabbed with Kimwipes to remove excess solution C. Slides were covered and left to dry for 1 week. Slides were developed according to the manufacturer's instructions and coverslipped with Permount (Electron microscopy Sciences, Hatfield, PA). Dendritic spine density analysis was performed using Neurolucida software (MBF Bioscience, Williston, VT) installed on a Zeiss Imager M.2 microscope.

Statistics.

GraphPad Prism v8 were used for all statistical analyses. All measurements were taken from distinct blinded samples. No statistical methods were used to pre-determine sample sizes but our sample sizes are similar to those reported in previous publications[2,3,12]. No data points were excluded from analysis. Data distribution was assumed to be normal but this was not formally tested. When comparing two conditions, unpaired two-tailed Student's t-test were used. When comparing more than two conditions, one-way ANOVA was performed, followed by two-tailed Dunnett's post-hoc test comparing all means to the control $SRPX2^{+/Y}$ mean. Axon segregation curves were analyzed with two-way ANOVA, with two-tailed Dunnett's post-hoc test. Sample sizes were estimated from previous publications. All images shown in figures are representative images of data quantified in the corresponding graphs.

Reporting Summary.

Further information on research design is available in the Nature Research Reporting Summary linked to this article.

Data availability.

The data that support the findings of this study are available from the corresponding author upon request.

Extended Data

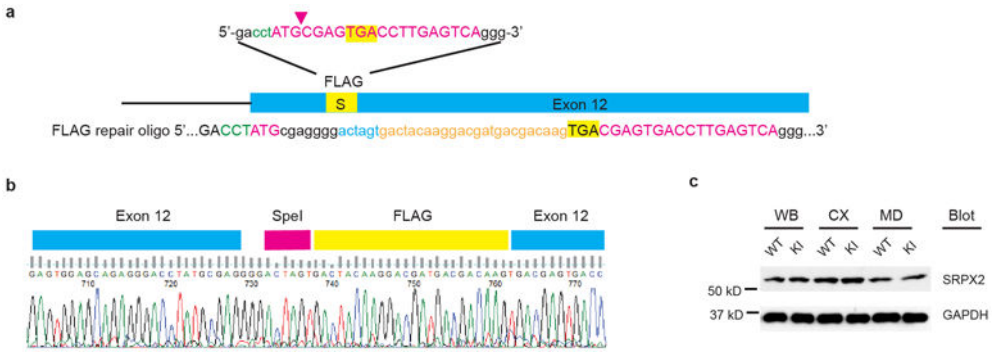

Extended Data Fig. 1 :

Author Manuscript Author Manuscript Author Manuscript Author Manuscript

a, Schematic of targeting site for SRPX2-FLAG KI mouse, depicting sgRNA sequences (magenta), PAM sequence (green), FLAG sequence (gold), restriction sites (blue), and stop codon (yellow). Arrow shows site of Cas9-induced double stranded break. **b**, Partial chromatograph of the genome sequence of the SRXP2-FLAG KI mouse, showing correct insertion of FLAG sequence. **c**, Western blot of SRPX2 from whole brain (WB), cortex (CX), and midbrain (MD) lysates from $SRPX2^{+/Y}$ and $SRPX2^{FLAG/Y}$ mouse brain, showing comparable amounts of endogenous SRPX2 in both genotypes. These experiments were repeated independently 3 times.

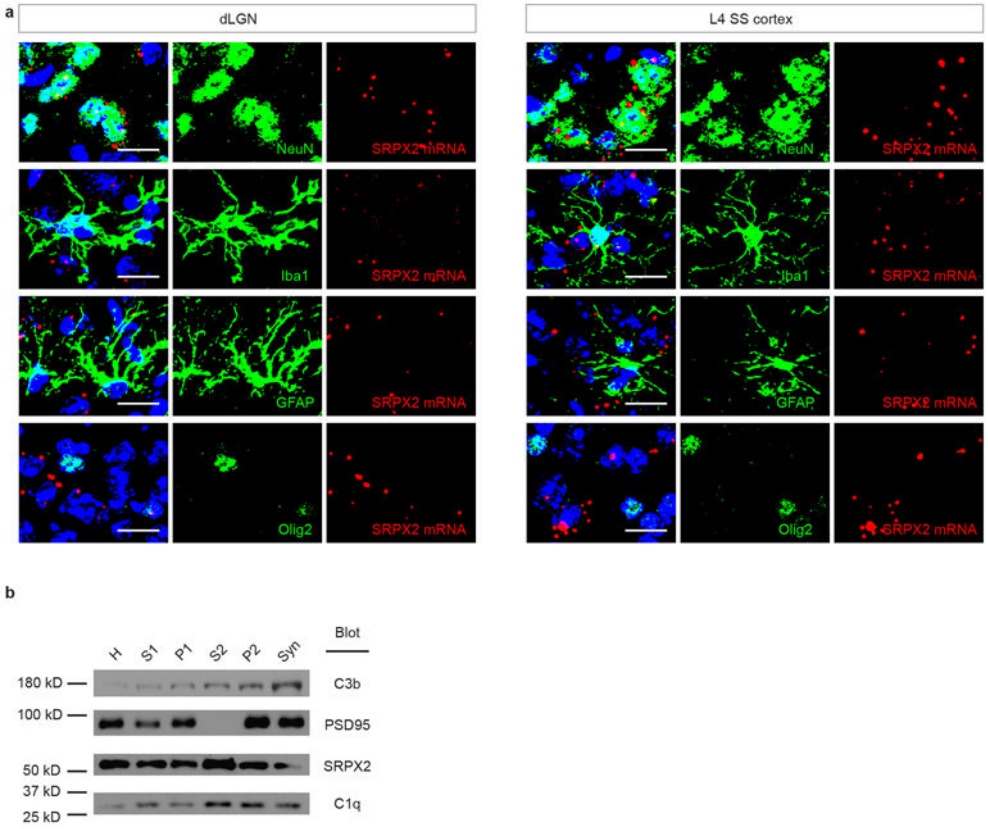

Extended Data Fig. 2 :

a, Representative images of RNAscope data presented in Fig. 2a, showing SRPX2 mRNA (red) and cell-specific markers NeuN/IbaI/GFAP/Olig2 (green) in separate channels for clarity. Nuclei were stained with DAPI (blue). Scale bar 20 μm. **b**, Synaptosome preparation from P60 mouse was immunoblotted for C3b, PSD95, SRPX2, and C1q. Fractions were brain homogenate (H), supernatant 1 (S1), pellet 1 (P1), supernatant 2 (S2), pellet 2 (P2) and synaptosomal fraction (Syn). This experiment was repeated independently 3 times.

Author Manuscript Author Manuscript Author Manuscript Author Manuscript

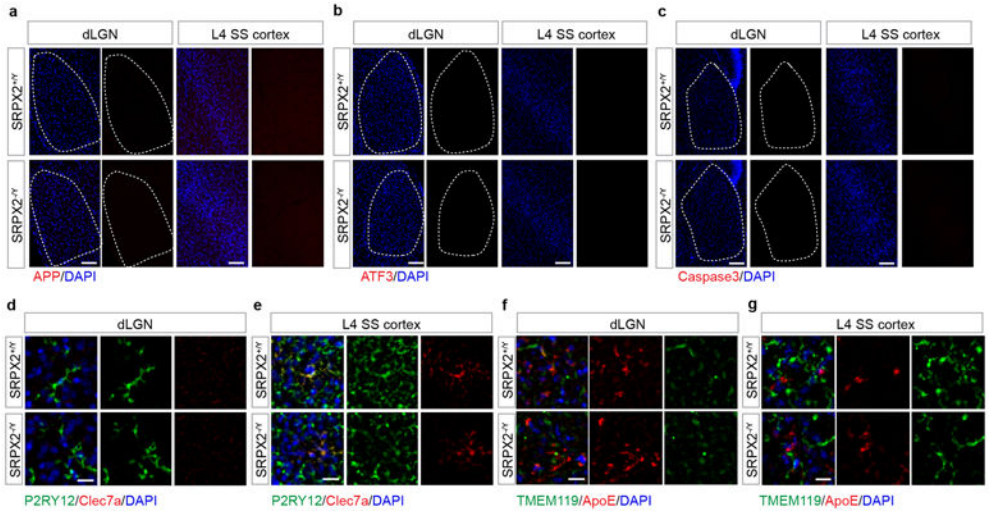

Extended Data Fig. 3 :

a-c, Representative images of P10 dLGN and P60 L4 SS cortex from SRPX2$^{+/Y}$ and SRPX2$^{-/Y}$ mice stained for neurodegeneration markers APP (**a**), ATF3 (**b**), and cleaved caspase 3 (**c**). Scale bar 100 μm. No staining for any neurodegeneration markers was observed in all mice. **d, e,** Representative images of P10 dLGN (**d**) and P60 L4 SS cortex (**e**) from SRPX2$^{+/Y}$ and SRPX2$^{-/Y}$ mice stained for microglial homeostatic state-associated marker P2RY12 and neurodegeneration state-associated marker Clec7a. Scale bar 10 μm. **f, g,** Representative images of P10 dLGN (**f**) and P60 L4 SS cortex (**g**) from SRPX2$^{+/Y}$ and SRPX2$^{-/Y}$ mice stained for microglial homeostatic state-associated marker TMEM119 and neurodegeneration state-associated marker ApoE. Scale bar 10 μm. Comparable levels of all microglial markers were present in SRPX2$^{+/Y}$ and SRPX2$^{-/Y}$ mice.

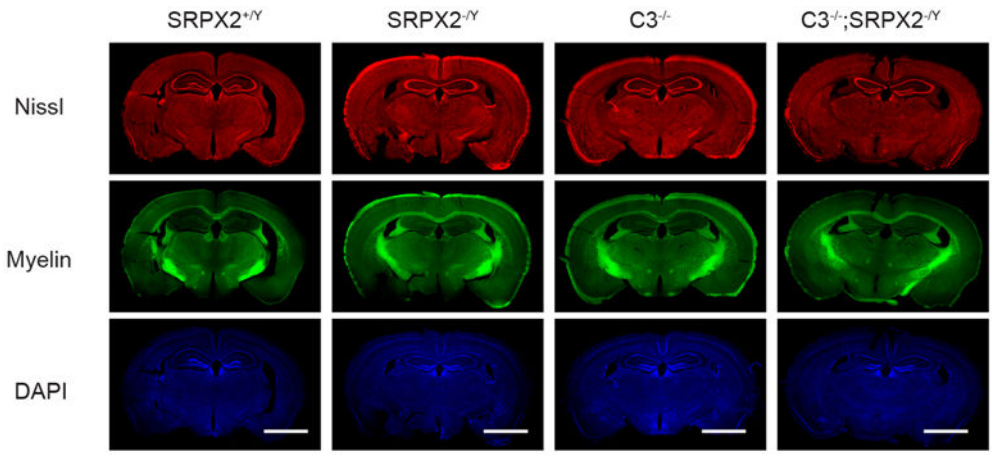

Extended Data Fig. 4 :

Representative images of coronal brain sections of P60 mice stained with Nissl, myelin, and DAPI stains with the BrainStain™ kit (Invitrogen). Scale bar 2000 μm.

Author Manuscript Author Manuscript Author Manuscript Author Manuscript

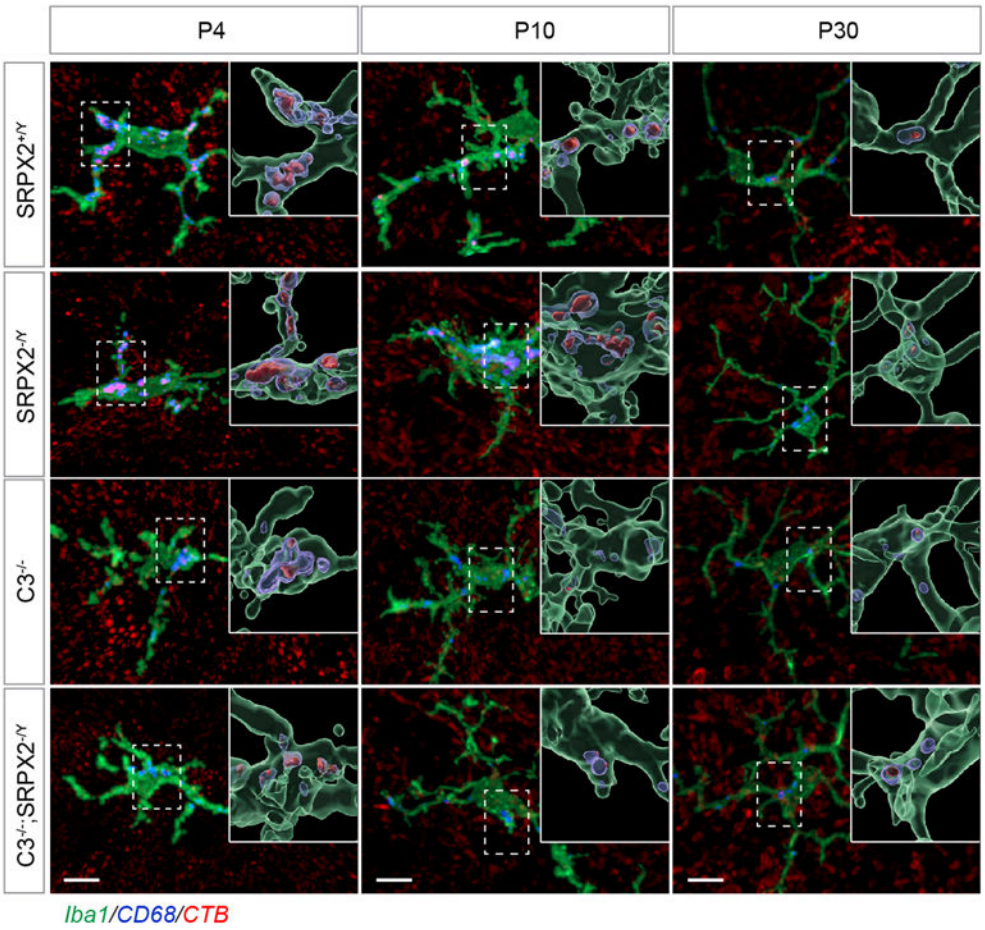

Extended Data Fig. 5 :

Representative images of microglial CTB engulfment in the dorsolateral geniculate nucleus at P4, P10 and P30. Inset shows 3D rendered engulfed CTB-labelled inputs (red) within CD68+ lysosomes (blue) in microglia (green). Scale bar 10 μm.

Author Manuscript Author Manuscript Author Manuscript Author Manuscript

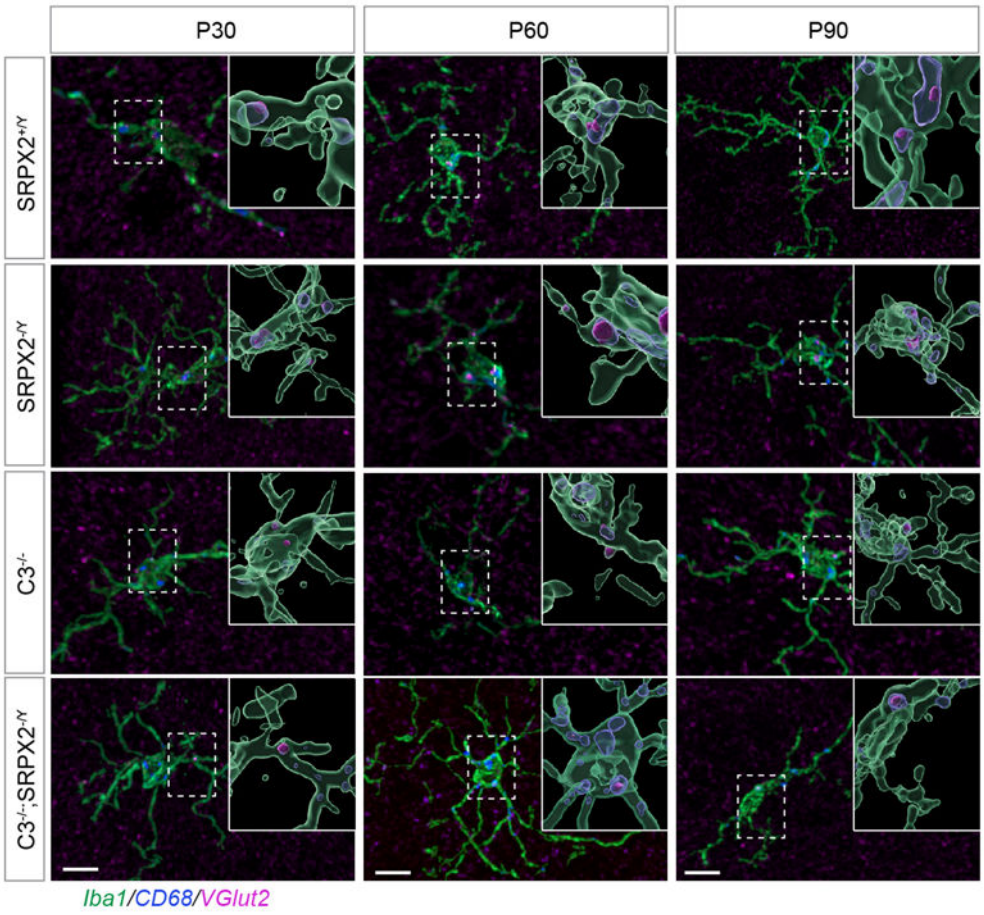

Extended Data Fig. 6 :

Representative fluorescence & 3D rendered images of microglia engulfing VGlut2 in L4 somatosensory cortex at P30, P60, P90. Inset shows engulfed VGlut2 (magenta) within microglial (green) CD68+ lysosomes (blue). Scale bar 10 μm.

ACKNOWLEDGEMENTS

We thank Dr. Andrea Tenner (UC Irvine) for complement-related reagents. We thank Dr. Daniel Lodge (UTHSCA) for use of his microscope system, and Dr. David Morilak (UTHSCSA) for use of histology equipment. We also thank Matthew Baum (Beth Steven's lab, Harvard) for technical advice on eye injections. CRISPR/Cas9 pronuclear injections were performed at the Johns Hopkins Transgenic Core Laboratory, and screening of founders and subsequent work was performed at UTHSCSA. This work was funded by the NARSAD Young Investigator grant number 25248 (G.M.S.), the William and Ella Owens Medical Research Foundation (G.M.S.), the Rising STARs award from the University of Texas System (G.M.S.), NINDS-R01NS112389 (G.M.S.), and NIDCD-R01DC03157 (J.H.K.). Images were generated at the Core Optical Imaging Facility which is supported by UTHSCSA, NCI-P30CA54174 (CTRC at UTHSCSA) and NIA-P01AG19316.

REFERENCES

1. Penzes P, Cahill ME, Jones KA, VanLeeuwen J-E & Woolfrey KM Dendritic spine pathology in neuropsychiatric disorders. Nat. Neurosci 14, 285–293 (2011). [PubMed: 21346746]
2. Stevens B et al. The classical complement cascade mediates CNS synapse elimination. Cell 131, 1164–78 (2007). [PubMed: 18083105]

Author Manuscript Author Manuscript Author Manuscript Author Manuscript

3. Schafer DP et al. Microglia sculpt postnatal neural circuits in an activity and complement-dependent manner. Neuron 74, 691–705 (2012). [PubMed: 22632727]
4. Chu Y et al. Enhanced synaptic connectivity and epilepsy in C1q knockout mice. Proc. Natl. Acad. Sci 107, 7975–7980 (2010). [PubMed: 20375278]
5. Hong S et al. Complement and microglia mediate early synapse loss in Alzheimer mouse models. Science 352, 712–716 (2016). [PubMed: 27033548]
6. Shi Q et al. Complement C3 deficiency protects against neurodegeneration in aged plaque-rich APP/PS1 mice. Sci. Transl. Med 9, (2017).
7. Lui H et al. Progranulin Deficiency Promotes Circuit-Specific Synaptic Pruning by Microglia via Complement Activation. Cell 0, (2016).
8. Simonetti M et al. Nuclear Calcium Signaling in Spinal Neurons Drives a Genomic Program Required for Persistent Inflammatory Pain. Neuron 77, 43–57 (2013). [PubMed: 23312515]
9. Vasek MJ et al. A complement–microglial axis drives synapse loss during virus-induced memory impairment. Nature 534, 538–543 (2016). [PubMed: 27337340]
10. Sekar A et al. Schizophrenia risk from complex variation of complement component 4. Nature 530, 177–183 (2016). [PubMed: 26814963]
11. Ricklin D, Hajishengallis G, Yang K & Lambris JD Complement - a key system for immune surveillance and homeostasis. Nat. Immunol 11, 785–797 (2010). [PubMed: 20720586]
12. Sia GM, Clem RL & Huganir RL The human language-associated gene SRPX2 regulates synapse formation and vocalization in mice. Science 342, 987–991 (2013). [PubMed: 24179158]
13. Chen XS et al. Next-generation DNA sequencing identifies novel gene variants and pathways involved in specific language impairment. Sci. Rep 7, 46105 (2017). [PubMed: 28440294]
14. Roll P et al. SRPX2 mutations in disorders of language cortex and cognition. Hum Mol Genet 15, 1195–207 (2006). [PubMed: 16497722]
15. Schirwani S, McConnell V, Willoughby J, DDD Study & Balasubramanian, M. Exploring the association between SRPX2 variants and neurodevelopment: How causal is it? Gene 685, 50–54 (2018). [PubMed: 30393191]
16. Soteros BM, Cong Q, Palmer CR & Sia GM Sociability and synapse subtype-specific defects in mice lacking SRPX2, a languageassociated gene. PloS One (2018).
17. Kirkitadze MD & Barlow PN Structure and flexibility of the multiple domain proteins that regulate complement activation. Immunol. Rev 180, 146–161 (2001). [PubMed: 11414356]
18. Håvik B et al. The complement control-related genes CSMD1 and CSMD2 associate to schizophrenia. Biol. Psychiatry 70, 35–42 (2011). [PubMed: 21439553]
19. Shimizu A et al. A novel giant gene CSMD3 encoding a protein with CUB and sushi multiple domains: a candidate gene for benign adult familial myoclonic epilepsy on human chromosome 8q23.3-q24.1. Biochem. Biophys. Res. Commun 309, 143–154 (2003). [PubMed: 12943675]
20. Yu Z-L et al. Febrile seizures are associated with mutation of seizure-related (SEZ) 6, a brain-specific gene. J. Neurosci. Res 85, 166–172 (2007). [PubMed: 17086543]
21. Stephan AH, Barres BA & Stevens B The Complement System: An Unexpected Role in Synaptic Pruning During Development and Disease. Annu. Rev. Neurosci 35, 369–389 (2012). [PubMed: 22715882]
22. Bally I et al. Expression of recombinant human complement C1q allows identification of the C1r/C1s-binding sites. Proc. Natl. Acad. Sci. U. S. A 110, 8650–8655 (2013). [PubMed: 23650384]
23. Holmquist E, Okroj M, Nodin B, Jirström K & Blom AM Sushi domain-containing protein 4 (SUSD4) inhibits complement by disrupting the formation of the classical C3 convertase. FASEB J 27, 2355–2366 (2013). [PubMed: 23482636]
24. Kölm R et al. Von Willebrand Factor Interacts with Surface-Bound C1q and Induces Platelet Rolling. J. Immunol. Baltim. Md 1950 197, 3669–3679 (2016).
25. Anwer M et al. Sushi repeat-containing protein X-Linked 2 - a novel phylogenetically conserved hypothalamo-pituitary protein. J. Comp. Neurol (2018) doi:10.1002/cne.24449.
26. Krasemann S et al. The TREM2-APOE Pathway Drives the Transcriptional Phenotype of Dysfunctional Microglia in Neurodegenerative Diseases. Immunity 47, 566–581.e9 (2017). [PubMed: 28930663]

Author Manuscript Author Manuscript Author Manuscript Author Manuscript

27. Chen C & Regehr WG Developmental remodeling of the retinogeniculate synapse. Neuron 28, 955–966 (2000). [PubMed: 11163279]
28. Lehrman EK et al. CD47 Protects Synapses from Excess Microglia-Mediated Pruning during Development. Neuron 100, 120–134.e6 (2018). [PubMed: 30308165]
29. Bialas AR & Stevens B TGF-β signaling regulates neuronal C1q expression and developmental synaptic refinement. Nat. Neurosci 16, 1773–1782 (2013). [PubMed: 24162655]
30. Petersen CCH The Functional Organization of the Barrel Cortex. Neuron 56, 339–355 (2007). [PubMed: 17964250]
31. Petreanu L, Mao T, Sternson SM & Svoboda K The subcellular organization of neocortical excitatory connections. Nature 457, 1142–1145 (2009). [PubMed: 19151697]
32. Oberlaender M et al. Cell type-specific three-dimensional structure of thalamocortical circuits in a column of rat vibrissal cortex. Cereb. Cortex N. Y. N 1991 22, 2375–2391 (2012).
33. Bian W-J, Miao W-Y, He S-J, Qiu Z & Yu X Coordinated Spine Pruning and Maturation Mediated by Inter-Spine Competition for Cadherin/Catenin Complexes. Cell 162, 808–822 (2015). [PubMed: 26255771]
34. Kraus DM et al. CSMD1 is a novel multiple domain complement-regulatory protein highly expressed in the central nervous system and epithelial tissues. J. Immunol. Baltim. Md 1950 176, 4419–4430 (2006).
35. Escudero-Esparza A, Kalchishkova N, Kurbasic E, Jiang WG & Blom AM The novel complement inhibitor human CUB and Sushi multiple domains 1 (CSMD1) protein promotes factor I-mediated degradation of C4b and C3b and inhibits the membrane attack complex assembly. FASEB J. Off. Publ. Fed. Am. Soc. Exp. Biol 27, 5083–5093 (2013).
36. Huberman AD, Feller MB & Chapman B Mechanisms Underlying Development of Visual Maps and Receptive Fields. Annu. Rev. Neurosci 31, 479–509 (2008). [PubMed: 18558864]
37. Bjartmar L et al. Neuronal Pentraxins Mediate Synaptic Refinement in the Developing Visual System. J. Neurosci 26, 6269–6281 (2006). [PubMed: 16763034]
38. Corriveau RA, Huh GS & Shatz CJ Regulation of class I MHC gene expression in the developing and mature CNS by neural activity. Neuron 21, 505–520 (1998). [PubMed: 9768838]
39. Huh GS et al. Functional requirement for class I MHC in CNS development and plasticity. Science 290, 2155–2159 (2000). [PubMed: 11118151]
40. Royer-Zemmour B et al. Epileptic and developmental disorders of the speech cortex: ligand/receptor interaction of wild-type and mutant SRPX2 with the plasminogen activator receptor uPAR. Hum Mol Genet 17, 3617–30 (2008). [PubMed: 18718938]
41. Salmi M et al. Tubacin prevents neuronal migration defects and epileptic activity caused by rat Srpx2 silencing in utero. Brain 136, 2457–2473 (2013). [PubMed: 23831613]
42. Huttenlocher PR Synaptic density in human frontal cortex - developmental changes and effects of aging. Brain Res. 163, 195–205 (1979). [PubMed: 427544]
43. Huttenlocher PR & Dabholkar AS Regional differences in synaptogenesis in human cerebral cortex. J. Comp. Neurol 387, 167–178 (1997). [PubMed: 9336221]
44. Petanjek Z et al. Extraordinary neoteny of synaptic spines in the human prefrontal cortex. Proc. Natl. Acad. Sci 108, 13281–13286 (2011). [PubMed: 21788513]
45. Rakic P, Bourgeois JP, Eckenhoff MF, Zecevic N & Goldman-Rakic PS Concurrent overproduction of synapses in diverse regions of the primate cerebral cortex. Science 232, 232–235 (1986). [PubMed: 3952506]
46. Pinto JGA, Jones DG & Murphy KM Comparing development of synaptic proteins in rat visual, somatosensory, and frontal cortex. Front. Neural Circuits 7, (2013).
47. Ma Y, Ramachandran A, Ford N, Parada I & Prince DA Remodeling of dendrites and spines in the C1q knockout model of genetic epilepsy. Epilepsia 54, 1232–1239 (2013). [PubMed: 23621154]
48. Gunner G et al. Sensory lesioning induces microglial synapse elimination via ADAM10 and fractalkine signaling. Nat. Neurosci 1 (2019) doi:10.1038/s41593-019-0419-y.
49. Welsh CA, Stephany C-É, Sapp RW & Stevens B Ocular dominance plasticity in binocular primary visual cortex does not require C1q. J. Neurosci (2019) doi:10.1523/JNEUROSCI.1011-19.2019.

Author Manuscript Author Manuscript Author Manuscript Author Manuscript

50. Harris CL, Heurich M, Cordoba S. R. de & Morgan BP The complotype: dictating risk for inflammation and infection. Trends Immunol. 33, 513–521 (2012). [PubMed: 22749446]

METHODS REFERENCES

51. Holmquist E, Okroj M, Nodin B, Jirström K & Blom AM Sushi domain-containing protein 4 (SUSD4) inhibits complement by disrupting the formation of the classical C3 convertase. FASEB J 27, 2355–2366 (2013). [PubMed: 23482636]

52. Turner JP & Salt TE Characterization of sensory and corticothalamic excitatory inputs to rat thalamocortical neurones in vitro. J Physiol 510, 829–843 (1998). [PubMed: 9660897]

53. Torborg CL & Feller MB Unbiased analysis of bulk axonal segregation patterns. J. Neurosci. Methods 135, 17–26 (2004). [PubMed: 15020085]

54. Torborg CL, Hansen KA & Feller MB High frequency, synchronized bursting drives eye-specific segregation of retinogeniculate projections. Nat. Neurosci 8, 72–78 (2005). [PubMed: 15608630]

55. Datwani A et al. Classical MHCI molecules regulate retinogeniculate refinement and limit ocular dominance plasticity. Neuron 64, 463–470 (2009). [PubMed: 19945389]

56. van Steensel B et al. Partial colocalization of glucocorticoid and mineralocorticoid receptors in discrete compartments in nuclei of rat hippocampus neurons. J. Cell. Sci 109 (Pt 4), 787–792 (1996). [PubMed: 8718670]

57. Bolte S & Cordelières FP A guided tour into subcellular colocalization analysis in light microscopy. Journal of Microscopy 224, 213–232 (2006). [PubMed: 17210054]

58. Guido W Development, form, and function of the mouse visual thalamus. J Neurophysiol 120, 211–225 (2018). [PubMed: 29641300]

59. Schafer DP, Lehrman EK, Heller CT, and Stevens B An engulfment assay: a protocol to assess interactions between CNS phagocytes and neurons. J Vis Exp. 88, 51482 (2014).

Author Manuscript Author Manuscript Author Manuscript Author Manuscript

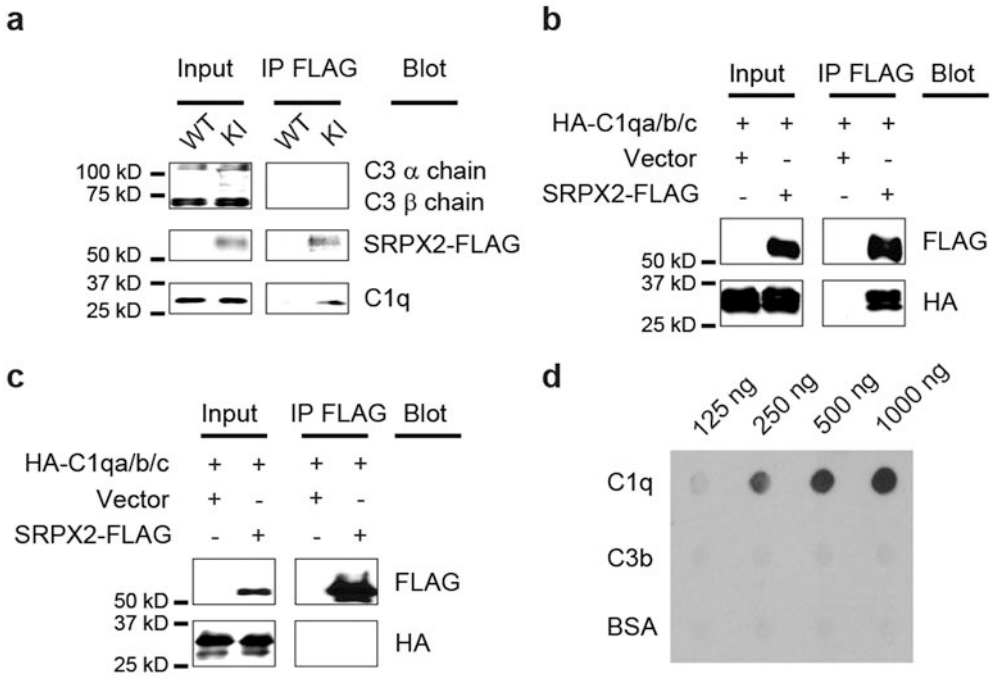

Fig. 1 : SRPX2 binds to C1q.

a, Immunoprecipitation (IP) of SRPX2-FLAG from mouse brain lysate co-immunoprecipitated C1q but not C3, which indicates that SRPX2 and C1q are present in the same protein complex in vivo in WT and SRPX2-FLAG knock-in (KI) mice. This experiment was repeated independently 4 times. **b**, HEK293 cells were cotransfected with SRPX2-FLAG and HA-C1q proteins, lysed, immunoprecipitated with an anti-FLAG antibody and blotted for HA and FLAG. Anti-FLAG beads immunoprecipitated murine C1qa/b/c only in the presence of SRPX2-FLAG. This experiment was repeated independently 4 times. **c**, HEK293T cells were co-transfected with SRPX2-FLAG and HA-C1q, and cell medium was collected. After clearing, the medium was immunoprecipitated with anti-FLAG antibody, and blotted for HA and FLAG. HA-C1q was not co-immunoprecipitated with SRPX2-FLAG from the cell medium. This experiment was independently repeated 3 times. **d**, Increasing amounts of purified C1q, C3b and BSA were immobilized onto a nitrocellulose membrane, which was then incubated with conditioned medium containing SRPX2-FLAG, and then blotted with anti-FLAG. SRPX2-FLAG shows dose-dependent saturable binding to purified human C1q, but not to C3b or BSA. This experiment was repeated independently 3 times.

Author Manuscript Author Manuscript Author Manuscript Author Manuscript

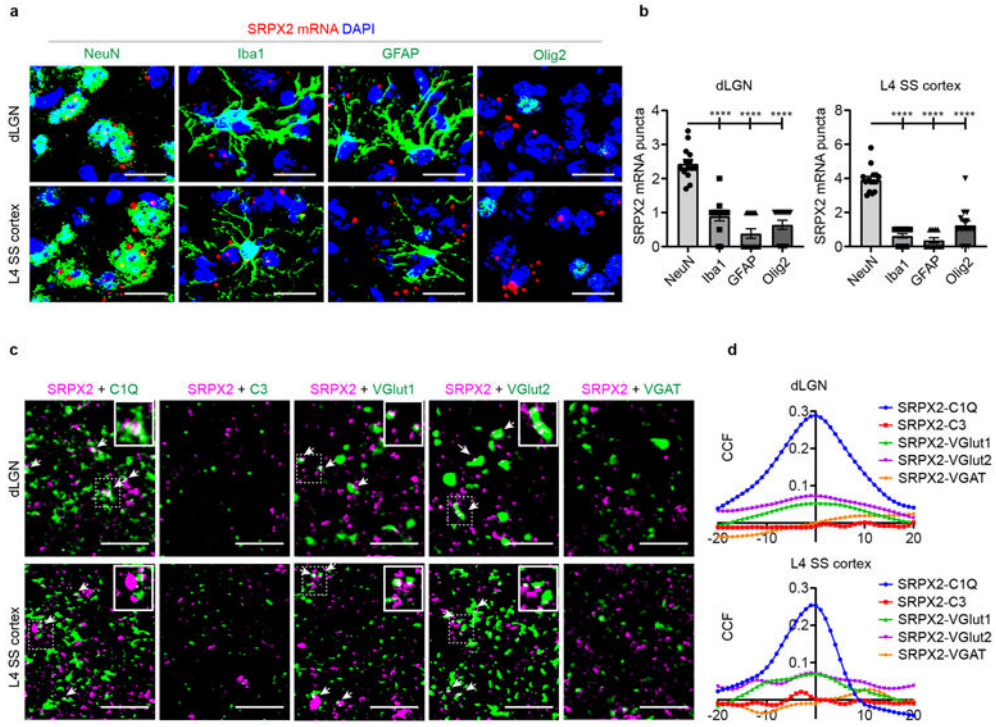

Fig. 2 : SRPX2 is expressed by neurons and colocalizes with C1q.

a, RNAscope ISH for *SRPX2* mRNA (red) in P10 dLGN and P60 L4 SS cortex, combined with immunostaining for cell-specific markers (green) for neurons (NeuN), microglia (Iba1), astrocytes (GFAP), and oligodendrocytes (Olig2). Nuclei were stained with DAPI (blue). Scale bars 20 μm. These experiments were repeated independently 4 times. **b,** Quantification of ISH for *SRPX2* mRNA in P10 dLGN and P60 L4 SS cortex. The number of SRPX2 mRNA puncta colocalized with the DAPI area of each cell type was plotted as mean ± s.e.m.. Data were analyzed using one-way ANOVA with two-sided Dunnett's post-hoc test comparing all means to NeuN. P10 dLGN: NeuN, $n = 14$, Iba1, $n = 13$ ****$P < 0.0001$, GFAP, $n = 13$ images ****$P < 0.0001$, Olig2, $n = 14$ ****$P < 0.0001$, all images from 3 mice each. P60 L4 of the SS cortex: NeuN, $n = 15$ images, Iba1, $n = 16$ images ****$P < 0.0001$, GFAP, $n = 11$ ****$P < 0.0001$, Olig2, $n = 15$ ****$P < 0.0001$;, all images from 3 mice each. **c**, Representative images of P10 LGN and P60 L4 SS cortex stained for SRPX2 (magenta) and complement components C1q and C3 (green), as well as synaptic markers VGlut1, VGlut2, and VGAT (green). Arrows indicate colocalized puncta of SRPX2 and C1q/VGlut1/VGlut2. Insets show magnified examples of colocalized puncta. Scale bars 10 μm. These experiments were repeated independently 3 times. **d,** Colocalization analysis of SRPX2 and various markers in P10 LGN and P60 L4 SS cortex. A Pearson's coefficient cross-correlation function (CCF) was calculated with the green channel shifted pixel by pixel with respect to the red channel. SRPX2 is most colocalized with C1q.

Author Manuscript Author Manuscript Author Manuscript Author Manuscript

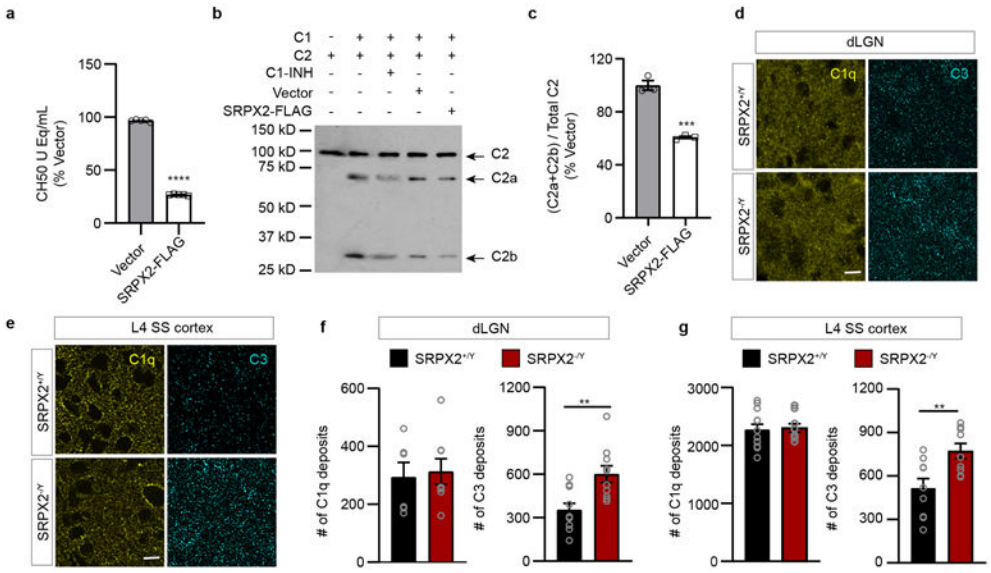

Fig. 3 : SRPX2 inhibits the classical complement pathway.

a, SRPX2 inhibition of complement activity was tested in the total complement activity (CH50) assay. SRPX2-FLAG immune-isolated from transfected HEK cells inhibited the generation of TCCs in normal human serum after activation of the classical complement pathway, as assessed using the CH50 enzyme-linked immunoassay (Quidel). Data are shown as mean ± s.e.m., and analyzed by two-tailed unpaired *t*-test, ****$P<0.0001$, n = 5. **b**, SRPX2-FLAG immune-isolated from transfected HEK293T cells was incubated with C1 and C2, and the cleavage of C2 was assessed by blotting for C2 fragments. As a negative control, C1 was omitted from the reaction. As a positive control for inhibition of C2 cleavage, a C1 inhibitor (C1-INH) was added. **c**, Intensities of bands representing cleaved C2 as a fraction of total C2 bands in the lane are plotted as means ± s.e.m., and analyzed by two-tailed unpaired *t*-test, ***$P = 0.0005$, n = 3. **d,e**, Representative images of P10 dLGN (**d**) and P60 L4 SS cortex (**e**) of *SRPX2*$^{+/Y}$ and *SRPX2*$^{-/Y}$ mice stained for C1q and C3. Scale bar 10 μm. These experiments were repeated independently 3-4 times. **f,g**, Quantitation of C1q and C3 levels in P10 dLGN (**f**) and P60 L4 SS cortex (**g**) of *SRPX2*$^{+/Y}$ and *SRPX2*$^{-/Y}$ mice. The total number of C1q/C3 particles are plotted as the mean ± s.e.m., and analyzed by two-tailed unpaired t test. For **f** (dLGN), C1q: *SRPX2*$^{+/Y}$, $n = 6$ from 3 mice, *SRPX2*$^{-/Y}$, $n = 8$ from 4 mice; C3: *SRPX2*$^{+/Y}$, $n = 10$, *SRPX2*$^{-/Y}$, $n = 10$, **$P = 0.0035$, both from 5 mice. For **g** (L4 SS cortex), C1q: *SRPX2*$^{+/Y}$, $n = 12$ from 4 mice, *SRPX2*$^{-/Y}$, $n = 9$ from 3 mice; C3: *SRPX2*$^{+/Y}$, $n = 9$, *SRPX2*$^{-/Y}$, $n = 9$, **$P = 0.0080$, both from 3 mice.

Author Manuscript Author Manuscript Author Manuscript Author Manuscript

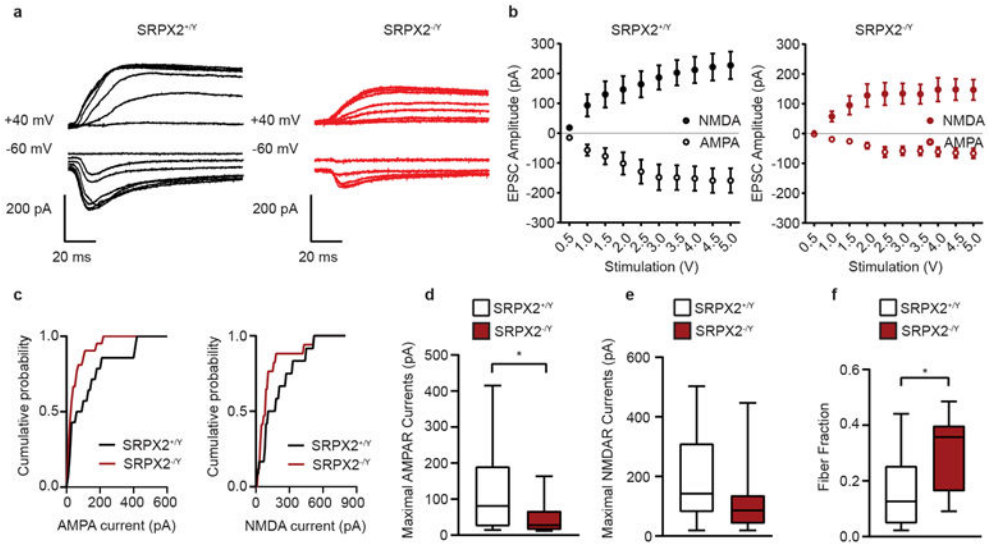

Fig. 4 : SRPX2 knockout reduces the number of functional inputs to dLGN neurons.

a, Representative whole-cell voltage-clamp neuron recordings from P10 parasagittal dLGN slices from *SRPX2*$^{+/Y}$ (left) and *SRPX2*$^{-/Y}$ mice (right), showing superimposed traces of excitatory postsynaptic currents (EPSCs) recorded in response to increasing stimulation of the optic tract at alternating holding potentials of −60 mV (AMPA receptor currents, inward) and +40 mV (combined AMPA and NMDA receptor currents, outward). **b**, The peaks of inward currents (open circles) and outward currents (filled circles) at various stimulus intensities were plotted as mean ± s.e.m., $n = 12$ cells from 7 mice; *SRPX2*$^{-/Y}$, $n = 21$ from 5 mice. **c**, Cumulative probability plots of amplitude for AMPA currents (left) and NMDA currents (right) in *SRPX2*$^{+/Y}$ and *SRPX2*$^{-/Y}$ mice. **d**, Maximal AMPA receptor (AMPAR) EPSCs were reduced in *SRPX2*$^{-/Y}$ mouse ($n = 21$ cells from 5 mice) relative to *SRPX2*$^{+/Y}$ mouse ($n = 14$ cells from 6 mice). Data were analyzed using two-tailed unpaired *t*-test, $*P = 0.0229$. **e**, Maximal NMDA receptor (NMDAR) EPSCs were not statistically different in *SRPX2*$^{-/Y}$ mouse ($n = 18$ cells from 7 mice) and *SRPX2*$^{+/Y}$ mouse ($n = 12$ cells from 5 mice). **f**, The FF of dLGN neurons was larger in *SRPX2*$^{-/Y}$ mouse ($n = 22$ cells from 7 mice) compared to *SRPX2*$^{+/Y}$ mouse ($n = 18$ cells from 5 mice), which indicates that there were fewer retinal inputs per dLGN neuron in the absence of SRPX2. Data were analyzed using two-tailed unpaired *t*-test, $*P = 0.0176$. For **d-f**, data are plotted as box plots, with the center line representing the median, the top and bottom of the box indicating the 25%-75% range, and the whiskers showing the 10-90% range.

Author Manuscript Author Manuscript Author Manuscript Author Manuscript

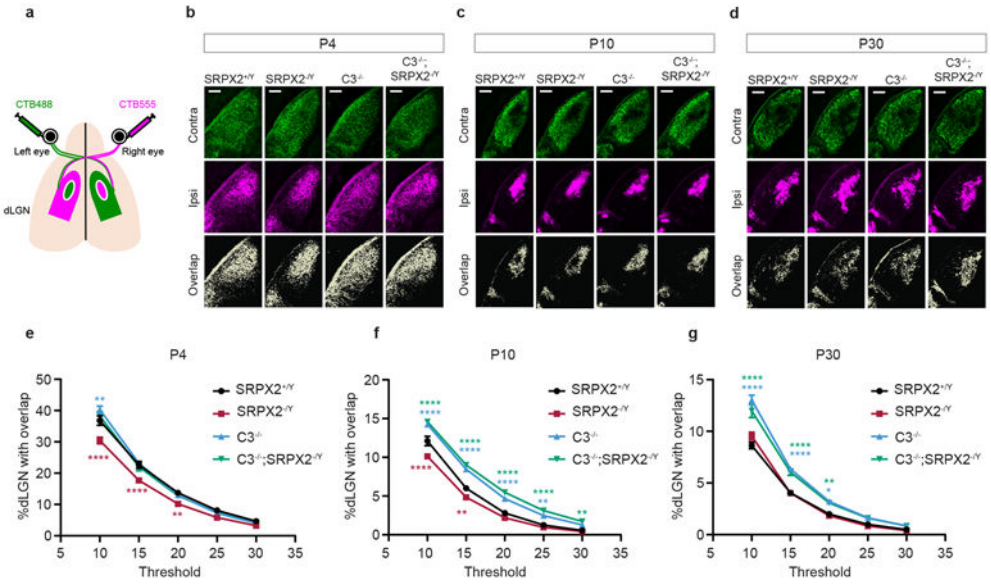

Fig. 5 : SRPX2 regulates complement-mediated RGC axon segregation in the dLGN.

a, Schematic of the retinogeniculate synapse elimination assay in dLGN. RGC afferents in dLGN were labelled by injecting CTβ-Alexa-488 and CTβ-Alexa-555 into the left eye and right eye respectively. **b-d** Representative P4 (**b**), P10 (**c**), and P30 (**d**) CTβ-labelled dLGN images. Contra, contralateral; ipsi, ipsilateral. Scale bars 200 μm. **e-g**, Multi-threshold analysis of percentage of P4 (**e**), P10 (**f**), and P30 (**g**) dLGN receiving inputs from both eyes. Data are plotted as mean ± s.e.m., and Analyzed using two-way ANOVA and two-tailed Dunnett's post-hoc test with means compared to $SRPX2^{+/Y}$. For **e** (P4): $SRPX2^{+/Y}$, $n = 6$ mice; $SRPX2^{-/Y}$, $n = 8$ mice; $C3^{-/-}$, $n = 7$ mice; $C3^{-/-}$; $SRPX2^{-/Y}$, $n = 5$ mice. at threshold 10, $SRPX2^{-/Y}$, $^{****}P < 0.000$; $C3^{-/-}$, $^{**}P = 0.0075$; at threshold 15, $SRPX2^{-/Y}$, $^{****}P < 0.0001$; at threshold 20, $SRPX2^{-/Y}$, $^{**}P = 0.0051$. For **f** (P10): $SRPX2^{+/Y}$, $n = 7$ mice; $SRPX2^{-/Y}$, $n = 7$ mice; $C3^{-/-}$, $n = 5$ mice; $C3^{-/-}$; $SRPX2^{-/Y}$, $n = 6$ mice. At threshold 10, $SRPX2^{-/Y}$ and $C3^{-/-}$ and $C3^{-/-}$; $SRPX2^{-/Y}$, $^{****}P < 0.0001$; at threshold 15, $SRPX2^{-/Y}$, $^{**}P = 0.0024$, $C3^{-/-}$ and $C3^{-/-}$; $SRPX2^{-/Y}$, $^{****}P < 0.0001$; at threshold 20, $C3^{-/-}$ and $C3^{-/-}$; $SRPX2^{-/Y}$, $^{****}P < 0.0001$; at threshold 25, $C3^{-/-}$, $^{**}P = 0.0043$, $C3^{-/-}$; $SRPX2^{-/Y}$, $^{****}P < 0.0001$; at threshold 30, $C3^{-/-}$; $SRPX2^{-/Y}$, $^{**}P = 0.0033$. For **g** (P30): $SRPX2^{+/Y}$, $n = 4$ mice; $SRPX2^{-/Y}$, $n = 4$ mice, $C3^{-/-}$, $n = 7$ mice; $C3^{-/-}$; $SRPX2^{-/Y}$, $n = 4$ mice. at thresholds 10 and 15, $C3^{-/-}$ and $C3^{-/-}$; $SRPX2^{-/Y}$, $^{****}P < 0.0001$; at threshold 20, $C3^{-/-}$, $^{**}P = 0.0019$, $C3^{-/-}$; $SRPX2^{-/Y}$, $^{*}P = 0.0184$.

Author Manuscript Author Manuscript Author Manuscript Author Manuscript

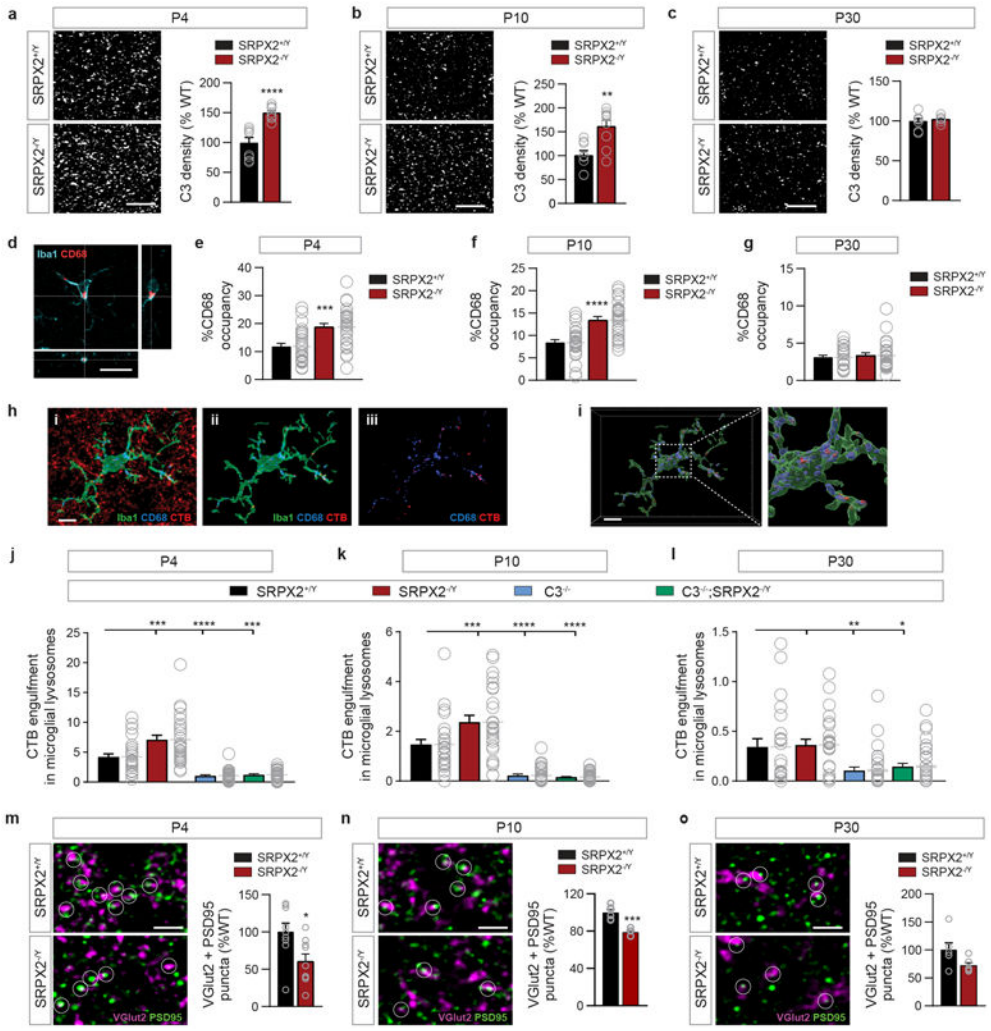

Fig. 6 : SRPX2 regulates complement-mediated microglial engulfment of synapses in the dLGN.

a-c, The dLGN of P4 (**a**), P10 (**b**), and P30 (**c**) *SRPX2*$^{+/Y}$ and *SRPX2*$^{-/Y}$ mice were immunostained for C3, and the number of C3 particles were quantitated. *SRPX2*$^{-/Y}$ mice showed elevated C3 deposition in the dLGN at P4 and P10 but not P30. Data are plotted as mean ± s.e.m., and Analyzed using two-tailed unpaired t test; *SRPX2*$^{+/Y}$, $n = 9$, *SRPX2*$^{-/Y}$, $n = 9$, $^{****}P < 0.0001$, both from 3 mice (**a**); *SRPX2*$^{+/Y}$, $n = 8$, *SRPX2*$^{-/Y}$, $n = 9$, $^{**}P = 0.0029$, both from 3 mice (**b**); *SRPX2*$^{+/Y}$, $n = 9$ from 3 mice, *SRPX2*$^{-/Y}$, $n = 6$ from 2 mice (**c**). Scale bars 10 μm. **d**, Orthogonal views of microglia staining, showing 3D colocalization of microglial marker Iba1 and lysosome marker CD68. Scale bar 10 μm. **e-g**, Quantitation of percentage of microglial volume containing CD68 in P4 (**e**), P10 (**f**) and P30 (**g**) mice. Data are plotted as the mean ± s.e.m., and Analyzed using two-tailed unpaired *t*-test; P4: *SRPX2*$^{+/Y}$, $n = 27$ cells, *SRPX2*$^{-/Y}$, $n = 30$ cells, $^{***}P = 0.0001$ (**e**); P10: *SRPX2*$^{+/Y}$, $n = 27$ cells, *SRPX2*$^{-/Y}$, $n = 26$ cells, $^{****}P < 0.0001$ (**f**); P30:, *SRPX2*$^{+/Y}$, $n = 23$ cells, *SRPX2*$^{-/Y}$, $n = 26$ cells, all from 3 mice each (**g**). **h,** Left: representative image of a microglia (green) from the dLGN of a P10 *SRPX2*$^{-/Y}$ mouse, with CD68+ lysosomes (blue) and CTβ–Alexa-555 (CTB)-labeled RGC inputs (red) from both eyes. Middle: microglia with background CTβ–Alexa-555 removed, showing lysosomes (blue) and engulfed RGC inputs

Author Manuscript Author Manuscript Author Manuscript Author Manuscript

(red). Right: image showing the microglia channel removed to visualize the localization of CTβ (red) to microglial lysosomes (blue). Scale bar, 10 μm. **j-l**, Quantitation of CTB engulfment within microglial lysosomes in P4 (**j**), P10 (**k**), and P30 (**l**) dLGN. Data are shown as mean ± s.e.m., and analyzed using one-way ANOVA with two-tailed Dunnett's post-hoc test, comparing means to $SRPX2^{+/Y}$. For **j** (P4): $SRPX2^{+/Y}$, $n = 27$, $SRPX2^{-/Y}$, $n = 28$, ***$P = 0.0002$, $C3^{-/-}$, $n = 26$, ****$P < 0.0001$, $C3^{-/-}$; $SRPX2^{-/Y}$, $n = 25$, ***$P = 0.0001$. For **k** (P10): $SRPX2^{+/Y}$, $n = 27$, $SRPX2^{-/Y}$, $n = 26$, ***$P = 0.0007$, $C3^{-/-}$, $n = 29$, ****$P < 0.0001$, $C3^{-/-}$; $SRPX2^{-/Y}$, $n = 33$, ****$P < 0.0001$. For **l** (P30): $SRPX2^{+/Y}$, $n = 23$, $SRPX2^{-/Y}$, $n = 26$, $P = 0.9875$, $C3^{-/-}$, $n = 32$, **$P = 0.0048$, $C3^{-/-}$; $SRPX2^{-/Y}$, $n = 33$, *$P = 0.0207$. All cells were from three mice per genotype. **m-o**, Left: the dLGN of P4 (**m**), P10 (**n**), d (**o**) $SRPX2^{+/Y}$ and $SRPX2^{-/Y}$ mice were immunostained for presynaptic and postsynaptic markers VGlut2 (magenta) and PSD95 (green). Circles indicate examples of colocalized pre- and postsynaptic puncta. Colocalized puncta were quantitated and plotted as the mean ± s.e.m., and analyzed using two-tailed unpaired *t*-test. For **m** (P4): $SRPX2^{+/Y}$, $n = 9$, $SRPX2^{-/Y}$, $n = 9$, *$P = 0.0223$. For **n** (P10): $SRPX2^{+/Y}$, $n = 6$, $SRPX2^{-/Y}$, $n = 5$, ***$P = 0.0003$. For **o** (P30): $SRPX2^{+/Y}$, $n = 6$, $SRPX2^{-/Y}$, $n = 6$. All measurements were from three mice each. Scale bars, 5 μm.

Author Manuscript Author Manuscript Author Manuscript Author Manuscript

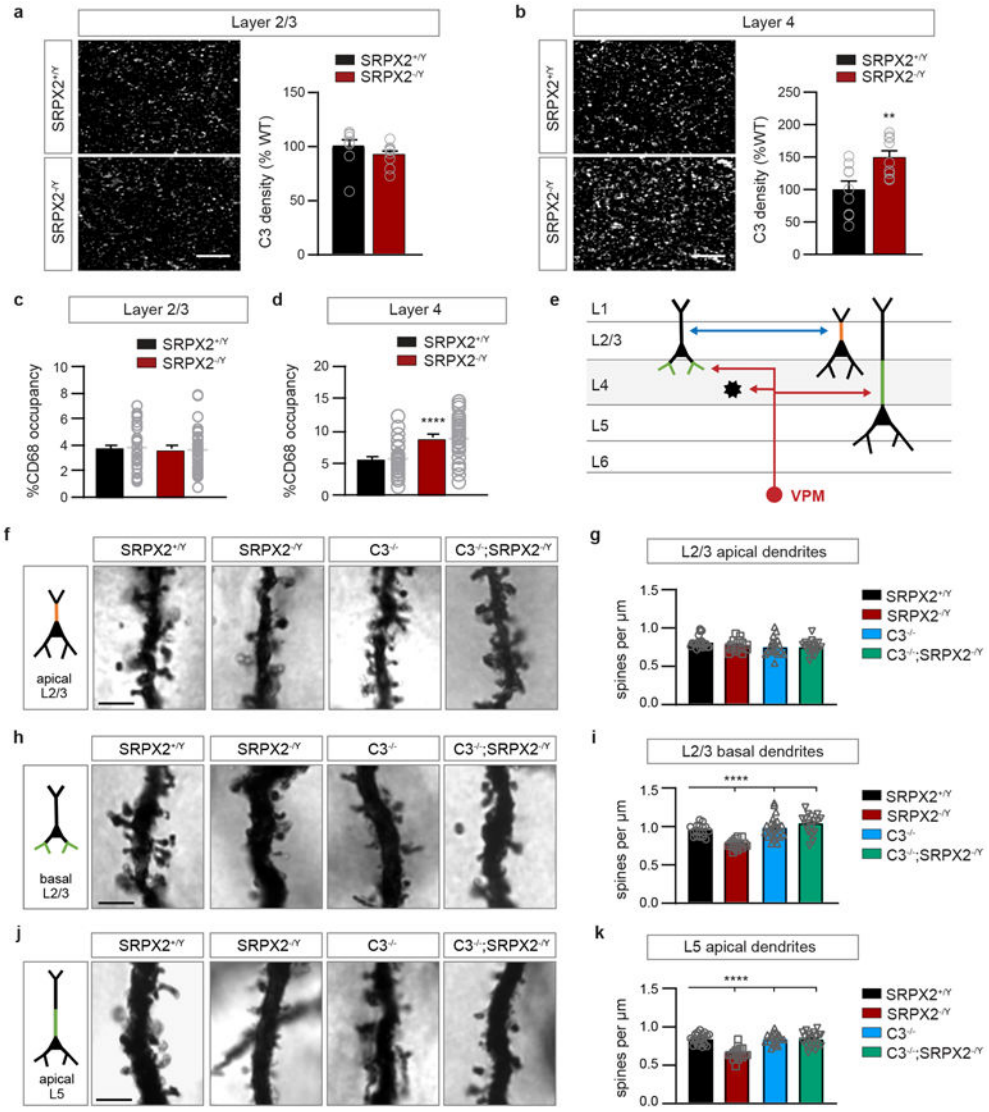

Fig. 7 : SRPX2 inhibits complement activation in L4 of the SS cortex but not L2/3.

a,b, The SS cortex of *SRPX2*$^{+/Y}$ and *SRPX2*$^{-/Y}$ mice were immunostained for C3, and the number of C3 particles in L2/3 (**a**) and L4 (**b**) were quantitated. *SRPX2*$^{-/Y}$ mice showed elevated C3 deposition in L4 but not L2/3. Data are plotted as mean ± s.e.m., and analyzed using two-tailed unpaired *t* test. For **a**, *SRPX2*$^{+/Y}$, $n = 8$, *SRPX2*$^{-/Y}$, $n = 9$. For **b**, *SRPX2*$^{+/Y}$, $n = 9$, *SRPX2*$^{-/Y}$, $n = 9$, $^{**}P = 0.008$. All measurements were from three mice each. Scale bars, 10 µm. **c,d,** Quantitation of the percentage of the microglial volume containing CD68 in L2/3 (**c**) and L4 (**d**). Data are plotted as mean ± s.e.m., and analyzed using two-tailed unpaired *t*-test. For **c**, *SRPX2*$^{+/Y}$, $n = 32$ cells, *SRPX2*$^{-/Y}$, $n = 34$ cells. For **d**, *SRPX2*$^{+/Y}$, $n = 30$, *SRPX2*$^{-/Y}$, $n = 34$ cells, $^{****}P < 0.0001$. All measurements were from three mice. **e,** Schematic of circuitry in the SS cortex, showing inputs from VPM thalamic afferents (red), and cortical afferents (blue). Dendrite segments within L4 from L5 and L2/3 neurons receiving thalamic inputs are highlighted in green, L4 stellate cells receiving thalamic inputs are depicted as a black star, and dendrite segments in L2/3

Author Manuscript Author Manuscript Author Manuscript Author Manuscript

receiving cortical inputs are highlighted in orange. **f,h,j** Representative images of Golgi-stained dendritic segments on L2/3 apical dendrites (**f**), L2/3 basal dendrites (**h**), and L5 apical dendrites (**j**). Scale bar 5 μm. **g,i,k** Quantification of dendritic spine density on apical L2/3 (**g**), basal L2/3 (**i**), and apical L5 (**k**) dendrites. Data are plotted as mean ± s.e.m., and analyzed using one-way ANOVA followed by two-tailed Dunnett's post-hoc test, comparing means to $SRPX2^{+/Y}$. For **g** (L2/3 apical dendrites): $SRPX2^{+/Y}$, $n = 20$, $SRPX2^{-/Y}$, $n = 17$, $C3^{-/-}$, $n = 18$, $C3^{-/-}$; $SRPX2^{-/Y}$, $n = 19$, all from 3 mice. For **i** (L2/3 basal dendrites): $SRPX2^{+/Y}$, $n = 16$, $SRPX2^{-/Y}$, $n = 16$, ****$P < 0.0001$, $C3^{-/-}$, $n = 23$, $C3^{-/-}$; $SRPX2^{-/Y}$, $n = 17$ from 3 mice each. For **k** (L5 apical dendrites): $SRPX2^{+/Y}$, $n = 21$, $SRPX2^{-/Y}$, $n = 18$, ****$P < 0.0001$, $C3^{-/-}$, $n = 18$, $C3^{-/-}$; $SRPX2^{-/Y}$, $n = 20$. All measurements were from three mice each.

Author Manuscript Author Manuscript Author Manuscript Author Manuscript

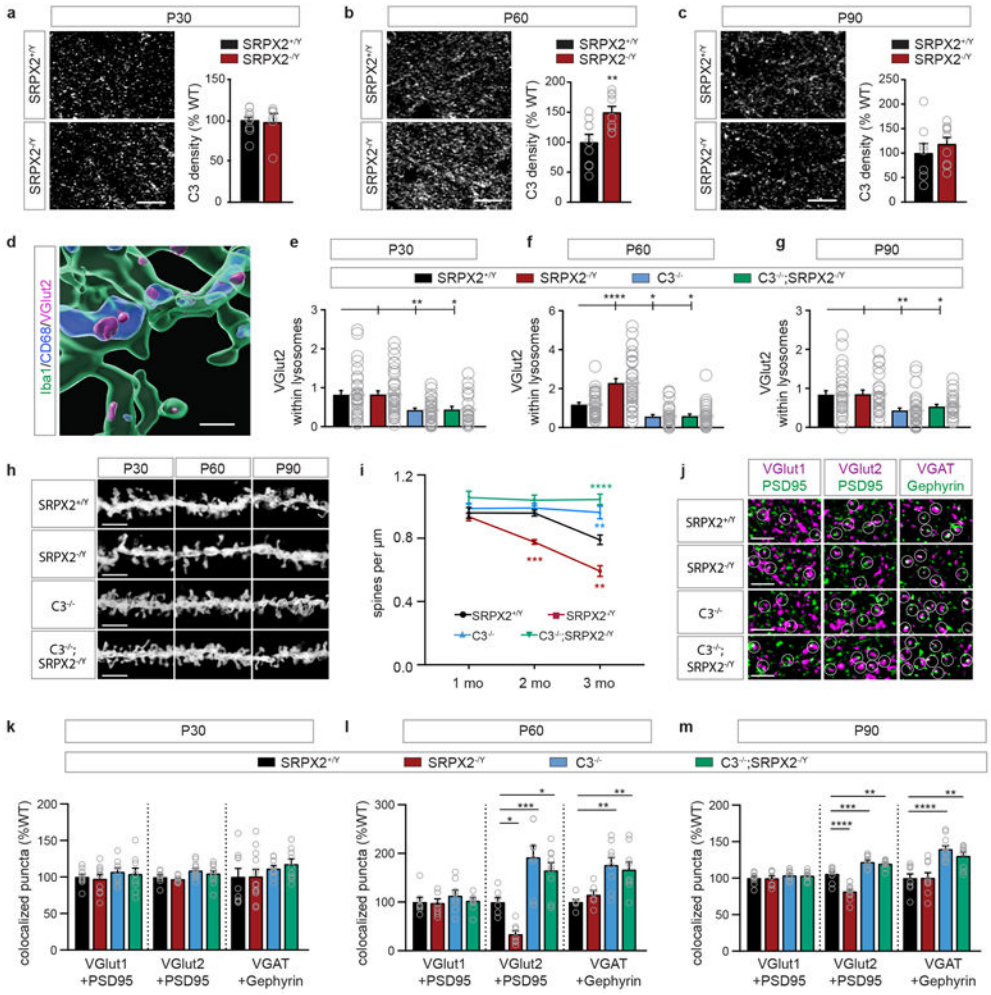

Fig. 8 : SRPX2 regulates complement-mediated synapse elimination in the SS cortex.

a-c, The L4 SS cortex of P30 (**a**), P60 (**b**) and P90 (**c**) *SRPX2*$^{+/Y}$ and *SRPX2*$^{-/Y}$ mice were immunostained for C3, and the number of C3 particles were quantitated. *SRPX2*$^{-/Y}$ mice showed elevated C3 deposition at P60 but not at P30 and P90. Note that the dataset for **b** is the same as that presented in Fig. 7b. The data are plotted as mean ± s.e.m,., and analyzed using two-tailed unpaired *t* test. For **a** (P30): $n = 9$ from 3 *SRPX2*$^{+/Y}$ mice, $n = 6$ from 2 *SRPX2*$^{-/Y}$ mice, $P = 0.9009$, $t(13)=0.1270$. For **b** (P60): $n = 9$ from 3 mice each, $^{**}P = 0.0080$, $t(16)=3.029$. For **c** (P90): $n = 9$ from 3 mice each, $P = 0.4446$, $t(16)=0.7838$. Scale bars, 10 µm. **d**, A Representative 3D reconstruction of microglia (green) showing localization of engulfed VGlut2 (magenta) in CD68+ lysosomes (blue). Scale bar 3 µm. **e-g** Quantitation of VGlut2 engulfment within microglial lysosomes in P30 (**e**), P60 (**f**), and P90 (**g**) L4 of the SS cortex. Data are shown as mean ± s.e.m., and analyzed using one-way ANOVA, followed by two-tailed Dunnett's post-hoc test, with the means compared to *SRPX2*$^{+/Y}$; For **e** (P30): *SRPX2*$^{+/Y}$, $n = 32$ cells; *SRPX2*$^{-/Y}$, $n = 35$ cells, $P > 0.9999$; *C3*$^{-/-}$, $n = 31$ cells, $^{**}P = 0.0056$; *C3*$^{-/-}$; *SRPX2*$^{-/Y}$, $n = 22$ cells, $^{*}P = 0.0162$. For (**f**) (P60): *SRPX2*$^{+/Y}$, $n = 30$ cells; *SRPX2*$^{-/Y}$, $n = 34$ cells, $^{****}P = 0.0001$; *C3*$^{-/-}$, $n = 26$ cells, $^{*}P = 0.0252$; *C3*$^{-/-}$; *SRPX2*$^{-/Y}$, $n = 30$ cells, $^{*}P = 0.0234$. For **g** (P90): *SRPX2*$^{+/Y}$, $n = 29$ cells; *SRPX2*$^{-/Y}$, $n = 22$ cells, $P = 0.9989$; *C3*$^{-/-}$, $n = 32$ cells, $^{**}P = 0.0017$; *C3*$^{-/-}$; *SRPX2*$^{-/Y}$, *n*

Author Manuscript Author Manuscript Author Manuscript Author Manuscript

= 25 cells, *P = 0.0403. All cells are from three mice per genotype. **h,** Representative inverted images of Golgi-stained secondary basal dendrites of L2/3 neurons located in L4 at P30, P60 and P90. Scale bar 5 μm. **i,** Quantitation of spine density of basal dendrites of L2/3 neurons in L4. Data are plotted as the mean ± s.e.m., and analyzed using two-way ANOVA followed by two-tailed Dunnett's post-hoc test, with the means compared to $SRPX2^{+/Y}$. P30: $SRPX2^{+/Y}$, n = 18, $SRPX2^{-/Y}$, n = 19, $C3^{-/-}$, n = 18, $C3^{-/-}$; $SRPX2^{-/Y}$, n = 15, all from 4 mice each. P60: $SRPX2^{+/Y}$, n = 16, $SRPX2^{-/Y}$, n = 16 ***P = 0.0006; $C3^{-/-}$, n = 23, P = 0.9951, $C3^{-/-}$; $SRPX2^{-/Y}$, n = 17 P = 0.4871, all from 3 mice each. P90: $SRPX2^{+/Y}$, n = 12, $SRPX2^{-/Y}$, n = 11, **P = 0.0024, $C3^{-/-}$, n = 18, **P = 0.0028, $C3^{-/-}$; $SRPX2^{-/Y}$, n = 12, ****P < 0.0001, all from 3 mice each. **j,** Representative images of colocalized synaptic puncta (VGlut1+PSD95, VGlut2+PSD95, and VGAT+gephyrin) in P60 L4 of the SS cortex. Presynaptic markers are in magenta, and postsynaptic markers in green. Circles indicate colocalized pre-and-post synaptic puncta. Scale bar 4 μm. **k-m** Quantification of colocalized pre-and-postsynaptic markers VGlut1+PSD95, VGlut2+PSD95, and VGAT+Gephyrin at P30 (**k**), P60 (**l**) and P90 (**m**). Data are shown as mean ± s.e.m., and analyzed using one-way ANOVA, followed by two-tailed Dunnett's post-hoc test, with the means compared to $SRPX2^{+/Y}$. For **k** (P30): VGlut1 + PSD95, $SRPX2^{+/Y}$, n = 9, $SRPX2^{-/Y}$, n = 10, $C3^{-/-}$, n = 9, $C3^{-/-}$; $SRPX2^{-/Y}$, n = 9, all from 3 mice; VGlut2 + PSD95, $SRPX2^{+/Y}$, n = 9, $SRPX2^{-/Y}$, n = 9, both from 3 mice, $C3^{-/-}$, n = 12, $C3^{-/-}$; $SRPX2^{-/Y}$, n = 12, both from 4 mice; VGAT + gephyrin, $SRPX2^{+/Y}$, n = 9 from 3 mice, $SRPX2^{-/Y}$, n = 12 from 4 mice, $C3^{-/-}$, n = 10 from 2 mice, $C3^{-/-}$; $SRPX2^{-/Y}$, n = 9 from 3 mice. For **l** (P60): VGlut1 + PSD95, $SRPX2^{+/Y}$, n = 7 from 2 mice, $SRPX2^{-/Y}$, n = 8 from 3 mice, $C3^{-/-}$, n = 8 from 3 mice, $C3^{-/-}$; $SRPX2^{-/Y}$, n = 9 from 3 mice; VGlut2 + PSD95, $SRPX2^{+/Y}$, n = 7 from 2 mice, $SRPX2^{-/Y}$, n = 9 from 3 mice, *P = 0.0158, $C3^{-/-}$, n = 8 from 3 mice, ***P = 0.0010, $C3^{-/-}$; $SRPX2^{-/Y}$, n = 9 from 3 mice, *P = 0.0165; VGAT + gephyrin, $SRPX2^{+/Y}$, n = 6 from 2 mice, $SRPX2^{-/Y}$, n = 6 from 2 mice, P = 0.8118, $C3^{-/-}$, n = 9 from 3 mice, **P = 0.0019, $C3^{-/-}$; $SRPX2^{-/Y}$, n = 9 from 3 mice, **P = 0.0064. For **m** (P90): VGlut1 + PSD95, $SRPX2^{+/Y}$, n = 9 from 3 mice, $SRPX2^{-/Y}$, n = 9 from 3 mice, $C3^{-/-}$, n = 12 from 4 mice, $C3^{-/-}$; $SRPX2^{-/Y}$, n = 9 from 3 mice; VGlut2 + PSD95, $SRPX2^{+/Y}$, n = 10 from 3 mice, $SRPX2^{-/Y}$, n = 12 from 4 mice, ****P < 0.0001, $C3^{-/-}$, n = 10 from 3 mice, ***P= 0.0002, $C3^{-/-}$; $SRPX2^{-/Y}$, n = 11 from 4 mice, **P = 0.0013; VGAT + gephyrin, $SRPX2^{+/Y}$, n = 9 from 3 mice, $SRPX2^{-/Y}$, n = 9 from 3 mice, P > 0.9999, $C3^{-/-}$, n = 11 from 4 mice, ****P < 0.0001, $C3^{-/-}$; $SRPX2^{-/Y}$, n = 9 from 3 mice, **P = 0.0025.